A novel constitutive model for surface elasticity at finite strains suitable across compressibility spectrum

Ali Javili[a,*], Berkin Dortdivanlioglu[c,b]

[a] *Department of Mechanical Engineering, Bilkent University, 06800 Ankara, Turkey*
[b] *Oden Institute for Computational Engineering and Sciences, The University of Texas at Austin, Austin, TX 78712, USA*
[c] *Department of Civil, Architectural and Environmental Engineering, The University of Texas at Austin, Austin, TX 78712, USA*

Abstract

The surface elasticity theory of Gurtin–Murdoch has proven to be remarkably successful in predicting the behavior of materials at the nano scale, which can be attributed to the fact that surface-to-volume increases as the problem dimension decreases. On the other hand, surface tension can deform *soft* elastic solids even at the macro scale resulting e.g. in elastocapillary instabilities in soft filaments reminiscent of Plateau–Rayleigh instabilities in fluids. Due to the increasing number of applications involving nanoscale structures and soft solids such as gels, the surface elasticity theory has experienced a prolific growth in the past two decades. Despite the large body of literature on the subject, the constitutive models of surface elasticity theory at large deformations is not suitable to capture the surface behavior from fully compressible to nearly incompressible elasticity, especially from a computational perspective. A physically meaningful and proper decomposition of the surface free energy density in terms of area-preserving and area-varying contributions remains yet to be established. We show that an immediate and intuitive generalization of the small-deformation surface constitutive models does not pass the simple extension test at large deformations and results in unphysical behavior at lower Poisson's ratios. Thus, the first contribution of the manuscript is to introduce a novel decomposed surface free energy density that recovers surface elasticity across the compressibility spectrum. The second objective of this paper is to formulate an axisymmetric counterpart of the elastocapillary theory methodically derived from its three-dimensional format based on meaningful measures relevant to the proposed surface elasticity model. Various aspects of the problem are elucidated and discussed through numerical examples using the finite element method enhanced with surface elasticity.

Keywords: Surface elasticity, Constitutive modeling, Axi-symmetric variational formulation

*Corresponding author.
Email addresses: ajavili@bilkent.edu.tr (Ali Javili), berkin@utexas.edu (Berkin Dortdivanlioglu)

1. Introduction

It is well known that the external surface of a continuous body has features that differ from those of the contained bulk. The growing surface-to-volume ratio at lower scales makes the impact of the boundary on the behavior of the material more evident, independent of the underlying physical composition. In addition to this, at macroscopic sizes, the surface energy of extremely soft solids such as gels is comparable to the bulk energy of elastic materials. As such, the elastocapillary effect emerges due to the energetic competition that takes place between the bulk and its boundary, which is immediately relevant to cavitation [1], soft composites behavior [2, 3], wetting on soft substrates [4–7], soft contact and adhesion [8, 9], fracture [10], capillary bending [11], and pattern formations in nature [12], to name few. A brief review of elastocapillary theory is given next.

The pioneering studies of Laplace, Young, and Gibbs shall be considered as the origins of both elastocapillary theory and surface modeling of continua. In line with Gibbsian thermodynamics and the influential work of Scriven [13], Gurtin and Murdoch [14] established a phenomenological surface elasticity model. This model has now been accepted for applications in nanomaterials, as shown in [15–19], among others. The assumption behind the surface elasticity theory is that a surface has its own tensorial stress, which may be derived from the surface constitutive laws. To be more specific, the surface has its own thermodynamic structure, and as a consequence, surface stresses are determined as energetically conjugated quantities to surface strains. The surface elasticity theory thus incorporates capillary effects as an essential component. Numerous analytical [15–18] and computational [20–22] studies have demonstrated that the size-dependent material response due to surface elasticity is physically meaningful and is also in agreement with atomistic simulations [23–26]. From a computational perspective, the finite element modeling of surface tension for *fluids* was carried by Saksono and Perić [27, 28] for quasi-static and dynamic problems, see also [29]. This formulation is suitable for fluids in that the surface tension is accounted for but the surface elasticity is absent. To address this issue, Yvonnet, *et al.* [20] introduced surface elasticity into the finite element method for *solids* though at *small strains* and in two dimensions only. Javili and Steinmann [30, 31] developed a finite element framework for continua with boundary energies that accounted for surface elasticity as well as surface tension for two-dimensional [30] and three-dimensional [31] solids at *finite deformations*. Henann and Bertoldi [32] employed this framework and established a numerical procedure appropriate for modeling elastocapillary phenomena using the commercial finite element (FE) package Abaqus and studied a variety of problems, see also [33]. A similar approach was adopted by Mora, *et al.* [34] and an ad-hoc approach using the FEniCS finite element library has been provided. He and Park [35] presented a computational methodology to capture elastocapillary, essentially equivalent to the classical Young–Laplace model, that could be readily incorporated to commercial FE packages such as ANSYS and COMSOL, see also [36]. The theory of surface elasticity has seen tremendous advancements in the last two decades [37], and the contributions

that have been listed here are only a few instances of the many more that have been made in this area. This renaissance of interest in the mechanics of solid surfaces may be primarily due to the advent of nanotechnology and the rising number of applications using soft solids such as gels. Other theoretical expansions of the idea have been offered from a theoretical perspective as well, see for example [38–43] among others.

In this contribution, we employ a completely variational elastocapillary theory at finite deformations that does not rely on the Young–Laplace equation. Specifically, unlike the usually accepted technique, which introduces surface tension ad hoc through an external force on the surface, we capture the surface tension via its energy representation. Thereby, surface tension is understood as a constant energy density per surface area in the spatial configuration that fits inherently in the variational framework. The methodology is specially valuable from a computational standpoint, and it furnishes an elegant framework for axisymmetric problems. Compared to earlier works on the topic, to the best of our knowledge, there are important areas where this study makes an original contribution to, as follows.

- We show that an intuitive generalization of the commonly accepted surface energy density [31] to decompose it to area-preserving and area-varying parts leads to unphysical results at low Poisson's ratios though it can be employed if we restricts ourselves to nearly incompressible surface behavior. To draw an analogy, we also show that various commonly accepted bulk free energy densities suffer from the same shortcoming, though frequently overlooked in literature.

- We propose an additive split of the hyperelastic surface energy density into area-preserving and area-varying parts, suitable for numerical treatment of nearly incompressible as well as compressible surface elasticity.

- We elaborate on how the isotropic surface elasticity parameters enter into degenerate three-dimensional cases such as axisymmetric problems. In doing so, we introduce a systematic treatment of elastocapillary for axisymmetric problems from its three-dimensional counterpart.

- The developed axisymmetric variational elastocapillary formulation is implemented employing surface-enriched finite elements assuming strongly coupled bulk and boundary deformations under large strain assumptions. Accompanying numerical examples illustrate the significance of the proposed surface elasticity model.

This manuscript is organized as follows. Section 2 lays the theoretical foundation for the study. First, the notation and definitions are introduced in Section 2.1. The kinematics of the problem is formulated and the key concepts of differential geometry required to describe the boundary motion are briefly reviewed in Section 2.2 followed by a generic framework suitable for a fully variational surface tension theory that is concisely formulated in Section 2.3. A more familiar three-dimensional problem is treated then in Section 3 to show the utility of proposed formulation and

consequently, its axisymmetric counterpart is established in Section 4. Thanks to the variational approach, the governing equations naturally emerge in their weak forms that are immediately suitable for computational implementation. The developed framework is elucidated via a series of numerical examples in Section 5. The numerical examples are devised such that both computational and physical aspects of the problem are covered. Section 6 concludes this work and provides an outlook for future work.

2. Theory

The purpose of this section is to briefly derive the governing equations of elasticity at finite deformations that account for surface tension as well as surface elasticity using a completely variational method in which the surface of a body has its own free energy density. We provide a formulation that establishes the governing equations in integral forms instantly suitable for computational implementation using the finite element method (FEM).

2.1. Notation and definitions

Direct notation is adopted throughout. Occasional use is made of index notation, the summation convention for repeated indices being implied. The scalar product of two vectors $\boldsymbol{a}$ and $\boldsymbol{b}$ is denoted $\boldsymbol{a} \cdot \boldsymbol{b} = [\boldsymbol{a}]_i[\boldsymbol{b}]_i$. The scalar product of two second-order tensors $\boldsymbol{A}$ and $\boldsymbol{B}$ is denoted $\boldsymbol{A} : \boldsymbol{B} = [\boldsymbol{A}]_{ij}[\boldsymbol{B}]_{ij}$. The composition of two second-order tensors $\boldsymbol{A}$ and $\boldsymbol{B}$, denoted $\boldsymbol{A}\cdot\boldsymbol{B}$, is a second-order tensor with components $[\boldsymbol{A}\cdot\boldsymbol{B}]_{ij} = [\boldsymbol{A}]_{is}[\boldsymbol{B}]_{sj}$. The surface quantities are distinguished from their bulk counterparts by an accent on top. That is, quantities or operators $\{\hat{\bullet}\}$ are the surface counterparts of the bulk quantity or operator $\{\bullet\}$, respectively, unless specified otherwise. The fourth-order identity tensor is denoted as $\mathbb{I}$. Similarly, other fourth-order constitutive tensors are also written with the same font, such as $\mathbb{A}$ for the fourth-order tangent tensor. The tensor product of two second-order tensors $\boldsymbol{A}$ and $\boldsymbol{B}$ is a fourth-order tensor $\mathbb{D} = \boldsymbol{A} \otimes \boldsymbol{B}$ with $[\mathbb{D}]_{ijkl} = [\boldsymbol{A}]_{ij}\,[\boldsymbol{B}]_{kl}$. The two non-standard tensor products of two second-order tensors $\boldsymbol{A}$ and $\boldsymbol{B}$ are the fourth-order tensors $[\boldsymbol{A}\overline{\otimes}\boldsymbol{B}]_{ijkl} = A_{ik}\,B_{jl}$ and $[\boldsymbol{A}\underline{\otimes}\boldsymbol{B}]_{ijkl} = A_{il}\,B_{jk}$.

2.2. Preliminaries

Consider the deformation of a continuum body, as illustrated in Fig. 1 that occupies the material configuration $\mathscr{B}_0 \subset \mathbb{R}^3$ at time $t = 0$ that is mapped to the spatial configuration $\mathscr{B}_t \subset \mathbb{R}^3$ at any time $t > 0$ via the nonlinear deformation map $\boldsymbol{\varphi}$ as

$$\boldsymbol{x} = \boldsymbol{\varphi}(\boldsymbol{X}, t) \;:\; \mathscr{B}_0 \times \mathbb{R}_+ \to \mathscr{B}_t \qquad \text{and} \qquad \hat{\boldsymbol{x}} = \boldsymbol{\varphi}(\hat{\boldsymbol{X}}, t) \;:\; \mathscr{S}_0 \times \mathbb{R}_+ \to \mathscr{S}_t\,, \tag{1}$$

with $\boldsymbol{X}$ and $\boldsymbol{x}$ identifying points in the material and spatial configurations, respectively. According to our convention, the surface quantities are denoted as $\{\hat{\bullet}\}$. That is, the placement of particles on the surface are labeled $\hat{\boldsymbol{X}}$ and $\hat{\boldsymbol{x}}$ in the material and spatial configurations, respectively, such that $\hat{\boldsymbol{X}} = \boldsymbol{X}|_{\mathscr{S}_0}$ and $\hat{\boldsymbol{x}} = \boldsymbol{x}|_{\mathscr{S}_t}$, where $\mathscr{S}_0 := \partial\mathscr{B}_0$ and $\mathscr{S}_t := \partial\mathscr{B}_t$. Central to the theory is the assumption that *the boundary is material* in the sense that the boundary is convected with the domain and remains perfectly bonded to the bulk throughout deformations, which is indicated via the surface mapping $(1)_2$. The deformation gradient in the bulk, denoted $\boldsymbol{F} := \mathrm{Grad}\boldsymbol{\varphi}$, is a linear deformation map that relates an infinitesimal line element $\mathrm{d}\boldsymbol{X} \in T\mathscr{B}_0$ to its spatial counterpart $\mathrm{d}\boldsymbol{x} \in T\mathscr{B}_t$ via the relation $\mathrm{d}\boldsymbol{x} = \boldsymbol{F} \cdot \mathrm{d}\boldsymbol{X}$. The gradient operator in the bulk in terms of the curvilinear coordinates ξ^i can be expressed as

$$\mathrm{Grad}\{\bullet\} := \frac{\partial\{\bullet\}}{\partial\xi^i} \otimes \boldsymbol{G}^i \qquad \text{and} \qquad \mathrm{grad}\{\bullet\} := \frac{\partial\{\bullet\}}{\partial\xi^i} \otimes \boldsymbol{g}^i \qquad \text{with} \qquad i \in \{1,2,3\}\,, \tag{2}$$

where $\boldsymbol{G}^i$ and $\boldsymbol{g}^i$ are the contravariant basis vectors in the material and spatial configurations, respectively. The contravariant vectors $\boldsymbol{G}^i$ and $\boldsymbol{g}^i$ form a dual basis to the covariant (natural) basis $\boldsymbol{G}_i$ and $\boldsymbol{g}_i$, in the material and spatial configurations, respectively. That is

$$\boldsymbol{G}_i := \frac{\partial\boldsymbol{X}}{\partial\xi^i} \quad \text{and} \quad \boldsymbol{g}_i := \frac{\partial\boldsymbol{x}}{\partial\xi^i} \qquad \Rightarrow \qquad \boldsymbol{G}_i \cdot \boldsymbol{G}^j = \delta_i^j \quad \text{and} \quad \boldsymbol{g}_i \cdot \boldsymbol{g}^j = \delta_i^j \qquad \text{with} \qquad \{i,j\} \in \{1,2,3\}\,, \tag{3}$$

where δ_i^j is the Kronecker delta. The deformation gradient therefore reads $\boldsymbol{F} = \boldsymbol{g}_i \otimes \boldsymbol{G}^i$ with its inverse defined as $\boldsymbol{f} := \boldsymbol{G}_i \otimes \boldsymbol{g}^i$. The properties $\boldsymbol{F} \cdot \boldsymbol{f} = \boldsymbol{i}$ and $\boldsymbol{f} \cdot \boldsymbol{F} = \boldsymbol{I}$ hold with $\boldsymbol{I}$ and $\boldsymbol{i}$ being the (mixed-variant) bulk identity tensors in the material and spatial configurations, respectively, as $\boldsymbol{I} := \boldsymbol{G}_i \otimes \boldsymbol{G}^i$ and $\boldsymbol{i} := \boldsymbol{g}_i \otimes \boldsymbol{g}^i$. See Fig. 1 (right) for a graphical illustration of the covariant basis vectors in the bulk and on the boundary. The ratio of the volume element in the spatial configuration $\mathrm{d}v$ over its counterpart in the material configuration $\mathrm{d}V$ is the Jacobian $J := \mathrm{d}v/\mathrm{d}V = \mathrm{Det}\boldsymbol{F}$. The surface $\mathscr{S}_0$ or $\mathscr{S}_t$ in the material or spatial configurations, respectively, is a two-dimensional manifold in the three-dimensional space $\mathbb{R}^3$ that can be parametrized in terms of two surface (curvilinear) coordinates $\hat{\xi}^\alpha$. The corresponding tangent vectors to the surface coordinate lines $\hat{\xi}^\alpha$, i.e. the covariant (natural) surface basis vectors, read

$$\hat{\boldsymbol{G}}_\alpha := \frac{\partial\hat{\boldsymbol{X}}}{\partial\hat{\xi}^\alpha} \quad \text{and} \quad \hat{\boldsymbol{g}}_\alpha := \frac{\partial\hat{\boldsymbol{x}}}{\partial\hat{\xi}^\alpha} \qquad \text{with} \qquad \alpha \in \{1,2\}\,, \tag{4}$$

in the material and spatial configurations, respectively. The surface contravariant vectors $\hat{\boldsymbol{G}}^\alpha$ and $\hat{\boldsymbol{g}}^\alpha$ form a dual basis to the covariant (natural) basis $\hat{\boldsymbol{G}}_\alpha$ and $\hat{\boldsymbol{g}}_\alpha$, in the material and spatial configurations, respectively. That is

$$\hat{\boldsymbol{G}}_\alpha \cdot \hat{\boldsymbol{G}}^\beta = \delta_\alpha^\beta \quad \text{and} \quad \hat{\boldsymbol{g}}_\alpha \cdot \hat{\boldsymbol{g}}^\beta = \delta_\alpha^\beta \qquad \text{with} \qquad \{\alpha,\beta\} \in \{1,2\}\,. \tag{5}$$

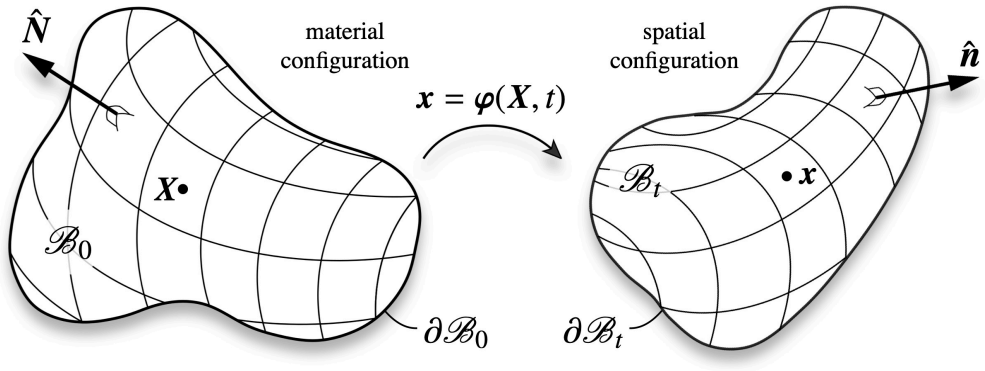

Figure 1: Finite deformation of a continuum body. The continuum body that occupies the material configuration $\mathscr{B}_0 \subset \mathbb{R}^3$ at time $t = 0$ is mapped to the spatial configuration $\mathscr{B}_t \subset \mathbb{R}^3$ via the nonlinear deformation map $\boldsymbol{\varphi}$. The boundary points are convected via the same deformation map $\boldsymbol{\varphi}$ as the bulk.

Similarly to the bulk, we define the surface deformation gradient $\hat{\boldsymbol{F}}$ as the linear map between the infinitesimal line element $\mathrm{d}\hat{\boldsymbol{X}} \in T\mathscr{S}_0$ and $\mathrm{d}\hat{\boldsymbol{x}} \in T\mathscr{S}_t$ with $\mathrm{d}\hat{\boldsymbol{x}} = \hat{\boldsymbol{F}} \cdot \mathrm{d}\hat{\boldsymbol{X}}$. The surface gradient operator reads

$$\hat{\mathrm{Grad}}\{\hat{\bullet}\} := \frac{\partial\{\hat{\bullet}\}}{\partial\hat{\xi}^\alpha} \otimes \hat{\boldsymbol{G}}^\alpha \qquad \text{and} \qquad \hat{\mathrm{grad}}\{\hat{\bullet}\} := \frac{\partial\{\hat{\bullet}\}}{\partial\hat{\xi}^\alpha} \otimes \hat{\boldsymbol{g}}^\alpha \qquad \text{with} \qquad \alpha \in \{1, 2\}\,. \tag{6}$$

Therefore, the surface deformation gradient $\hat{\boldsymbol{F}} := \hat{\boldsymbol{g}}_\alpha \otimes \hat{\boldsymbol{G}}^\alpha$ and its inverse $\hat{\boldsymbol{f}} := \hat{\boldsymbol{G}}_\alpha \otimes \hat{\boldsymbol{g}}^\alpha$ possess the properties $\hat{\boldsymbol{F}} \cdot \hat{\boldsymbol{f}} = \hat{\boldsymbol{i}}$ and $\hat{\boldsymbol{f}} \cdot \hat{\boldsymbol{F}} = \hat{\boldsymbol{I}}$ with $\hat{\boldsymbol{I}}$ and $\hat{\boldsymbol{i}}$ being the surface identity tensors in the material and spatial configurations, respectively. In contrast to the bulk, the surface identities $\hat{\boldsymbol{I}}$ and $\hat{\boldsymbol{i}}$ are not equal since $\hat{\boldsymbol{I}} := \hat{\boldsymbol{G}}_\alpha \otimes \hat{\boldsymbol{G}}^\alpha = \boldsymbol{I} - \hat{\boldsymbol{N}} \otimes \hat{\boldsymbol{N}}$ and $\hat{\boldsymbol{i}} := \hat{\boldsymbol{g}}_\alpha \otimes \hat{\boldsymbol{g}}^\alpha = \boldsymbol{i} - \hat{\boldsymbol{n}} \otimes \hat{\boldsymbol{n}}$ where $\hat{\boldsymbol{N}}$ and $\hat{\boldsymbol{n}}$ denote the unit vector orthogonal to the surface in the material and spatial configurations, respectively. The ratios of area elements in the spatial over the material configuration is defined by $\hat{J}$, as $\hat{J} := \mathrm{d}a/\mathrm{d}A$ which is the surface determinant of $\hat{\boldsymbol{F}}$ though, in contrast to the bulk, $\hat{\boldsymbol{F}}$ is rank-deficient and thus, its determinant is non-standard. The bulk and surface determinant operators in the material configuration are defined in a unified manner as

$$\begin{aligned} \mathrm{Det}\{\bullet\} &:= \frac{|\,[\{\bullet\} \cdot \boldsymbol{G}_1] \cdot [\,[\{\bullet\} \cdot \boldsymbol{G}_2] \times [\{\bullet\} \cdot \boldsymbol{G}_3]\,]\,|}{|\,\boldsymbol{G}_1 \cdot [\boldsymbol{G}_2 \times \boldsymbol{G}_3]\,|} \qquad \Rightarrow \qquad J := \mathrm{Det}\boldsymbol{F} = \frac{|\,\boldsymbol{g}_1 \cdot [\,\boldsymbol{g}_2 \times \boldsymbol{g}_3\,]\,|}{|\,\boldsymbol{G}_1 \cdot [\boldsymbol{G}_2 \times \boldsymbol{G}_3]\,|}\,, \\ \hat{\mathrm{Det}}\{\hat{\bullet}\} &:= \frac{|\,[\{\hat{\bullet}\} \cdot \hat{\boldsymbol{G}}_1] \times [\{\hat{\bullet}\} \cdot \hat{\boldsymbol{G}}_2]\,|}{|\,\hat{\boldsymbol{G}}_1 \times \hat{\boldsymbol{G}}_2\,|} \qquad \Rightarrow \qquad \hat{J} := \hat{\mathrm{Det}}\hat{\boldsymbol{F}} = \frac{|\,\hat{\boldsymbol{g}}_1 \times \hat{\boldsymbol{g}}_2\,|}{|\,\hat{\boldsymbol{G}}_1 \times \hat{\boldsymbol{G}}_2\,|}\,. \end{aligned} \tag{7}$$

2.3. Generic framework

The objective of this section is to derive the governing equations of a continuum body accounting for surface tension in a variationally consistent framework. The choice of a variational structure is particularly helpful since (i) it immediately allows for an elegant axisymmetric formulation, devoid of external contributions and (ii) it intrinsically

results in governing equations in their (weak) integral form directly suitable for computational implementation in that Young–Laplace equation does not explicitly appear throughout the manuscript and thus, the surface curvature and surface divergence operator remain embedded in the framework without emerging in the derivations. In order to obtain the governing equations, the total energy functional is minimized. The total energy functional Ψ consists of the internal and external contributions denoted Ψ^{int} and Ψ^{ext}, respectively. To minimize Ψ, its first variation is set to zero as $\delta\Psi = \delta\Psi^{\text{int}} + \delta\Psi^{\text{ext}} \doteq 0$. The (incremental) external energy here Ψ^{ext} is essentially minus (incremental) working, i.e. $\delta\Psi^{\text{ext}} = -\delta\mathcal{W}$. For the sake of brevity, we leave out the external energy in the derivations assuming that (i) the body forces vanish, (ii) $\delta\boldsymbol{\varphi}$ is zero where displacements are prescribed and (iii) $\boldsymbol{t}_0$ is zero everywhere that a Neumann-type boundary condition is imposed. The latter is possible since *here, the surface tension is not treated on ad-hoc basis via an externally prescribed traction on the surface, but instead, it is captured within the internal energy density of the surface*. The (internal) energy $\Psi^{\text{int}} \equiv \Psi$ is composed of bulk and surface contributions. Let ψ denote the bulk free energy density per volume in the material configuration and $\hat{\psi}$ denote the surface free energy density per area in the spatial configuration. Therefore, from a variational perspective, equilibrium for the current problem reduces to

$$\delta\Psi = \int_{\mathscr{B}_0} \delta\psi \,\mathrm{d}V + \int_{\partial\mathscr{B}_0} \delta\hat{\psi} \,\mathrm{d}A \doteq 0 \quad \Rightarrow \quad \int_{\mathscr{B}_0} \frac{\partial\psi}{\partial\boldsymbol{\varphi}} \cdot \delta\boldsymbol{\varphi} \,\mathrm{d}V + \int_{\partial\mathscr{B}_0} \frac{\partial\hat{\psi}}{\partial\boldsymbol{\varphi}} \cdot \delta\boldsymbol{\varphi} \,\mathrm{d}A \doteq 0 \quad \forall\delta\boldsymbol{\varphi} \in \mathscr{H}_0^1(\mathscr{B}_0)\,. \tag{8}$$

The arbitrary motion variations $\delta\boldsymbol{\varphi}$ in the context of FEM can be expressed in their discretized form as $\delta\boldsymbol{\varphi} = N^i\,\delta\boldsymbol{\varphi}^i$, with N^i being the shape function associated with the "control" point i. That is

$$\int_{\mathscr{B}_0} \frac{\partial\psi}{\partial\boldsymbol{\varphi}^i} \cdot \delta\boldsymbol{\varphi}^i \,\mathrm{d}V + \int_{\partial\mathscr{B}_0} \frac{\partial\hat{\psi}}{\partial\boldsymbol{\varphi}^i} \cdot \delta\boldsymbol{\varphi}^i \,\mathrm{d}A \doteq 0 \qquad \forall\delta\boldsymbol{\varphi}^i \in \mathscr{H}_0^1(\mathscr{B}_0)\,. \tag{9}$$

Due to the arbitrariness of $\delta\boldsymbol{\varphi}^i$, Eq. (9) can be *formally* expressed as $\boldsymbol{R}^I \cdot \delta\boldsymbol{\varphi}^I \doteq 0$ for all arbitrary $\delta\boldsymbol{\varphi}^I$ which immediately implies $\boldsymbol{R}^I \doteq \boldsymbol{0}$ with $\boldsymbol{R}^I = \mathbf{A}\,\boldsymbol{R}^i$. Here $\boldsymbol{R}^i$ is the point-wise residual at point i associated with its global number I and $\mathbf{A}$ is the assembly operator. That is, we seek for the solutions of

$$\boldsymbol{R}^I \doteq \boldsymbol{0} \qquad \text{with} \qquad \boldsymbol{R}^I := \int_{\mathscr{B}_0} \frac{\partial\psi}{\partial\boldsymbol{\varphi}^i} \,\mathrm{d}V + \int_{\partial\mathscr{B}_0} \frac{\partial\hat{\psi}}{\partial\boldsymbol{\varphi}^i} \,\mathrm{d}A\,. \tag{10}$$

The residual vector is obviously composed of the residuals in the bulk and the residuals on the surface. Equation (10) is the point of departure for the remaining discussions. Note that Eq. (10) is essentially a nonlinear system of equations composed of DOFs relations, with DOFs being the number of degrees of freedom. For nonlinear problems at large deformations, the deformation is computed incrementally. To solve the nonlinear system of equations (10), at each increment, an iterative Newton–Raphson scheme is utilized. The global residual $\boldsymbol{R}$ is set to zero at (the end of) each

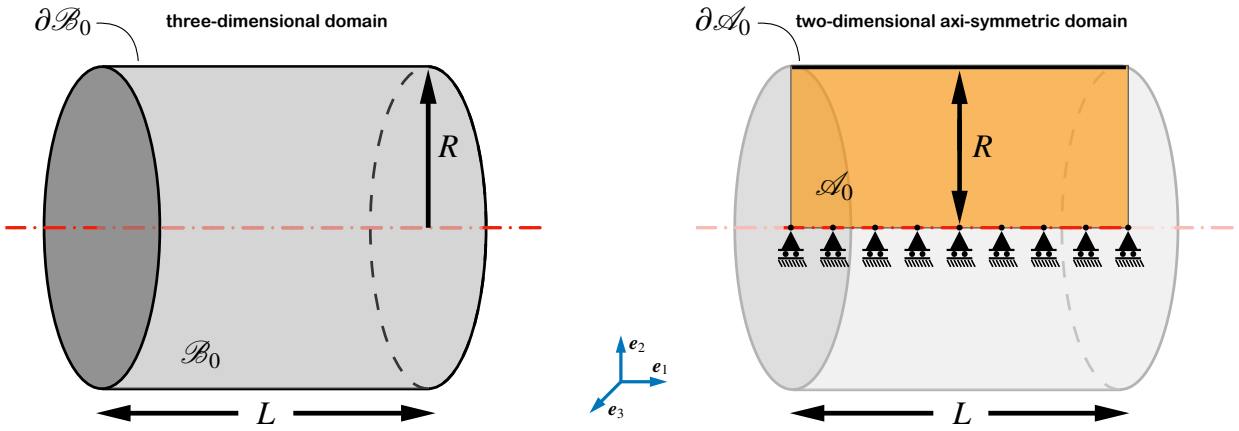

Figure 2: The geometry of the domain in the material configuration. Due to the axisymmetric nature of the problem, the three-dimensional domain $\mathscr{B}_0$ (left) reduces to the two-dimensional domain $\mathscr{A}_0$ (right). The two-dimensional surface $\partial\mathscr{B}_0$ of the three-dimensional domain therefore becomes a one-dimensional line $\partial\mathscr{A}_0$ on the two-dimensional domain.

increment resulting in the consistent linearization of the resulting system of equations at any iteration k

$$\boldsymbol{R}^I(\boldsymbol{\varphi}_{k+1}) \doteq \boldsymbol{0} \qquad \text{and} \qquad \boldsymbol{R}^I(\boldsymbol{\varphi}_{k+1}) = \boldsymbol{R}^I(\boldsymbol{\varphi}_k) + \boldsymbol{K}^{IJ}\big|_k \cdot \Delta\boldsymbol{\varphi}_k^J \doteq \boldsymbol{0} \qquad \text{with} \qquad \boldsymbol{K}^{IJ} := \frac{\partial \boldsymbol{R}^I}{\partial \boldsymbol{\varphi}^J}\,, \tag{11}$$

where $\boldsymbol{K}^{IJ}$ is the tangent stiffness at any $\boldsymbol{\varphi}_k$. Then the global deformation is updated at each iteration according to $\boldsymbol{\varphi}_{k+1} = \boldsymbol{\varphi}_k + \Delta\boldsymbol{\varphi}_k$ until the norm of the residual vector reaches zero, numerically speaking.

Equipped with the preliminaries, next we formulate the residual and stiffness for both a fully three-dimensional description as well as its axisymmetric counterpart. When dealing with the axisymmetric case, without loss of generality, we assume that the out-of-plane coordinate is the third one. That is, the "two-dimensional" domain corresponding to an axisymmetric problem is on the plane orthogonal to $\boldsymbol{e}_3$. The height of a point on the two-dimensional domain is its vertical distance from the symmetry axis as $H := \boldsymbol{X} \cdot \boldsymbol{e}_2$ and $h := \boldsymbol{x} \cdot \boldsymbol{e}_2$ in the material and spatial configurations, respectively. In the three-dimensional setting, the free energy density in the bulk per unit volume in the material configuration, denoted as ψ, will be a function of the deformation gradient as $\psi = \psi(\boldsymbol{F})$. For the axisymmetric problem though, it will become a function of in-plane deformation gradient $\mathcal{F}$ and out-of-plane component of the deformation gradient ζ with $\zeta = h/H$. That is

$$\boldsymbol{F} = \boldsymbol{g}_i \otimes \boldsymbol{G}^i \quad \text{and} \quad i \in \{1,2,3\} \qquad \Rightarrow \qquad \boldsymbol{F} = \mathcal{F} + \zeta\, \boldsymbol{e}_3 \otimes \boldsymbol{e}_3 \quad \text{with} \quad \mathcal{F} = \boldsymbol{g}_j \otimes \boldsymbol{G}^j \quad \text{and} \quad j \in \{1,2\}\,. \tag{12}$$

The free energy density of the surface per unit area in the material configuration, denoted as $\hat{\psi}$, will be a function of the surface deformation gradient as $\hat{\psi} = \hat{\psi}(\hat{\boldsymbol{F}})$. For the axisymmetric case, the surface deformation gradient is

decomposed into its in-plane part $\hat{\boldsymbol{\mathcal{F}}}$ and out-of-plane component $\hat{\zeta}$, analogous to the bulk. That is

$$\hat{\boldsymbol{F}} = \hat{\boldsymbol{g}}_\alpha \otimes \hat{\boldsymbol{G}}^\alpha \quad \text{and} \quad \alpha \in \{1,2\} \qquad \Rightarrow \qquad \hat{\boldsymbol{F}} = \hat{\boldsymbol{\mathcal{F}}} + \hat{\zeta}\, \boldsymbol{e}_3 \otimes \boldsymbol{e}_3 \qquad \text{with} \qquad \hat{\boldsymbol{\mathcal{F}}} = \hat{\boldsymbol{g}}_\alpha \otimes \hat{\boldsymbol{G}}^\alpha \quad \text{and} \quad \alpha \in \{1\}\,, \tag{13}$$

wherein $\hat{\zeta} = \hat{h}/\hat{H}$. Finally, we define the in-plane identity tensor $\boldsymbol{\mathcal{I}}$ and out-of-plane identity tensors $\boldsymbol{\mathcal{I}}_\perp$ as $\boldsymbol{\mathcal{I}} := \boldsymbol{G}_j \otimes \boldsymbol{G}^j$ and $\boldsymbol{\mathcal{I}}_\perp := \boldsymbol{e}_3 \otimes \boldsymbol{e}_3 = \boldsymbol{I} - \boldsymbol{\mathcal{I}}$ with $j \in \{1,2\}$ with their surface counterparts $\hat{\boldsymbol{\mathcal{I}}} := \hat{\boldsymbol{G}}_\alpha \otimes \hat{\boldsymbol{G}}^\alpha$ and $\hat{\boldsymbol{\mathcal{I}}}_\perp := \boldsymbol{e}_3 \otimes \boldsymbol{e}_3 = \hat{\boldsymbol{I}} - \hat{\boldsymbol{\mathcal{I}}}$, respectively.

3. Three-dimensional formulation

In this section, we briefly provide an overview of the three-dimensional formulation with focus on constitutive modeling and in particular on additive decomposition of free energy densities in the bulk and on the surface in Sections 3.1 and 3.2, respectively. In doing so, we derive the residual and stiffness for a fully three-dimensional description. The (internal) energy that we seek to minimize reads

$$\Psi = \int_{\mathscr{B}_0} \psi \, \mathrm{d}V + \int_{\partial\mathscr{B}_0} \hat{\psi} \, \mathrm{d}A \qquad \text{with} \qquad \psi = \psi(\boldsymbol{F}) \quad \text{and} \quad \hat{\psi} = \hat{\psi}(\hat{\boldsymbol{F}})\,, \tag{14}$$

where $\boldsymbol{F} = \boldsymbol{g}_i \otimes \boldsymbol{G}^i$ and $\hat{\boldsymbol{F}} = \hat{\boldsymbol{g}}_\alpha \otimes \hat{\boldsymbol{G}}^\alpha$. Therefore, the residual (10) follows from the chain rule as

$$\boldsymbol{R}^I = \int_{\mathscr{B}_0} \boldsymbol{P} : \frac{\partial \boldsymbol{F}}{\partial \boldsymbol{\varphi}^i} \, \mathrm{d}V + \int_{\mathscr{B}_0} \hat{\boldsymbol{P}} : \frac{\partial \hat{\boldsymbol{F}}}{\partial \boldsymbol{\varphi}^i} \, \mathrm{d}A\,, \tag{15}$$

with Piola stresses in the bulk and on the surface defined by $\boldsymbol{P} := \partial\psi/\partial\boldsymbol{F}$ and $\hat{\boldsymbol{P}} := \partial\hat{\psi}/\partial\hat{\boldsymbol{F}}$, respectively. The discretized forms of the deformation gradients follow using the shape functions as

$$\text{in } \mathscr{B}_0 \quad : \quad \boldsymbol{\varphi} = N^i \boldsymbol{\varphi}^i \quad \Rightarrow \quad \boldsymbol{F} = \boldsymbol{\varphi}^i \otimes \mathrm{Grad} N^i \quad , \quad \text{on } \partial\mathscr{B}_0 \quad : \quad \boldsymbol{\varphi} = \hat{N}^i \boldsymbol{\varphi}^i \quad \Rightarrow \quad \hat{\boldsymbol{F}} = \boldsymbol{\varphi}^i \otimes \hat{\mathrm{Grad}} \hat{N}^i\,. \tag{16}$$

Note that N^i and $\hat{N}^i$ are the shape functions in the bulk and on the surface respectively. Consequently, the derivatives of the deformation gradient with respect to the discretized motion in Eq. (15) in the bulk and on the surface read

$$\begin{aligned}
&\frac{\partial \boldsymbol{F}}{\partial \boldsymbol{\varphi}^i} = \frac{\partial}{\partial \boldsymbol{\varphi}^i} \left(\boldsymbol{\varphi}^s \otimes \mathrm{Grad} N^s\right) = \frac{\partial \boldsymbol{\varphi}^s}{\partial \boldsymbol{\varphi}^i} \,\overline{\otimes}\, \mathrm{Grad} N^s = \delta_{si}\, \boldsymbol{i} \,\overline{\otimes}\, \mathrm{Grad} N^s \qquad \Rightarrow \qquad \frac{\partial \boldsymbol{F}}{\partial \boldsymbol{\varphi}^i} = \boldsymbol{i} \,\overline{\otimes}\, \mathrm{Grad} N^i\,, \\
&\frac{\partial \hat{\boldsymbol{F}}}{\partial \boldsymbol{\varphi}^i} = \frac{\partial}{\partial \boldsymbol{\varphi}^i} \left(\boldsymbol{\varphi}^s \otimes \hat{\mathrm{Grad}} \hat{N}^s\right) = \frac{\partial \boldsymbol{\varphi}^s}{\partial \boldsymbol{\varphi}^i} \,\overline{\otimes}\, \hat{\mathrm{Grad}} \hat{N}^s = \delta_{si}\, \boldsymbol{i} \,\overline{\otimes}\, \hat{\mathrm{Grad}} \hat{N}^s \qquad \Rightarrow \qquad \frac{\partial \hat{\boldsymbol{F}}}{\partial \boldsymbol{\varphi}^i} = \boldsymbol{i} \,\overline{\otimes}\, \hat{\mathrm{Grad}} \hat{N}^i\,.
\end{aligned} \tag{17}$$

Inserting the derivatives $(17)_1$ and $(17)_2$ in Eq. (15) immediately furnishes

$$\boldsymbol{R}^I = \int_{\mathscr{B}_0} \boldsymbol{P} \cdot \mathrm{Grad} N^i \, \mathrm{d}V + \int_{\mathscr{B}_0} \hat{\boldsymbol{P}} \cdot \hat{\mathrm{Grad}} \hat{N}^i \, \mathrm{d}A \,. \tag{18}$$

Assuming that the global point J corresponds to its element-wise number j, using the chain-rule with $\mathbb{A} := \partial \boldsymbol{P} / \partial \boldsymbol{F}$ and $\hat{\mathbb{A}} := \partial \hat{\boldsymbol{P}} / \partial \hat{\boldsymbol{F}}$, and employing the relations (17), the tangent stiffness is then computed as

$$\boldsymbol{K}^{IJ} = \frac{\partial \boldsymbol{R}^I}{\partial \boldsymbol{\varphi}^J} = \int_{\mathscr{B}_0} \mathrm{Grad} N^i \mathbin{\bar{\cdot}} \mathbb{A} \cdot \mathrm{Grad} N^j \, \mathrm{d}V + \int_{\mathscr{B}_0} \hat{\mathrm{Grad}} N^i \mathbin{\bar{\cdot}} \hat{\mathbb{A}} \cdot \hat{\mathrm{Grad}} N^j \, \mathrm{d}A \,. \tag{19}$$

wherein $\bar{\cdot}$ is a non-standard contraction that is introduced for the sake of brevity as

$$[\mathrm{Grad} N^i \mathbin{\bar{\cdot}} \mathbb{A} \cdot \mathrm{Grad} N^j]_{ac} = [\mathrm{Grad} N^i]_b [\mathbb{A}]_{abcd} [\mathrm{Grad} N^j]_d \,. \tag{20}$$

Having established the final format for the residual (18), the last step is to set the free energy densities ψ in the bulk in Section 3.1 and $\hat{\psi}$ on the surface in Section 3.2 .

3.1. Constitutive modeling of the bulk

In order to set the stage and to explain a fundamental issue associated with commonly accepted free energy densities that employ additive decomposition, gathered in Fig. 3, we briefly deal with classical *three-dimensional* isotropic elasticity in the bulk first. This fundamental issue can be stated as follows. *If the free energy density of the bulk is decomposed into volume-preserving and volumetric parts, the material behavior may not pass the simple extension test at low Poisson's ratios in that e.g. it results in lateral expansion under uniaxial tension even for simple (non-auxetic) materials.* Thus, additional care must be taken when proposing such decomposed energy densities. Somewhat surprisingly, this issue is frequently overlooked in literature although it has been reported in [44] and even more recently in [45], see also [46] and for further details including an elaborate discussion on Baker–Ericksen inequality, see [47] among others.

Before illustrating the issue for various commonly accepted energy densities and providing a solution, we focus on a particular energy density to highlight the problem. The frequently employed Flory-type free energy density reads

$$\psi = \frac{1}{2} \mu \, [\, J^{-\frac{2}{3}} \, \boldsymbol{F} : \boldsymbol{F} - 3 \,] + \frac{1}{2} \kappa \, [\, \log J \,]^2 \qquad \text{with} \qquad J = \mathrm{Det} \boldsymbol{F} \,, \tag{21}$$

in which μ and κ are the shear and bulk moduli, respectively. For three-dimensional isotropic elasticity, the Poisson ratio ν can be related to μ and κ. Furthermore, for non-auxetic materials corresponding to $\nu \geq 0$ translates into

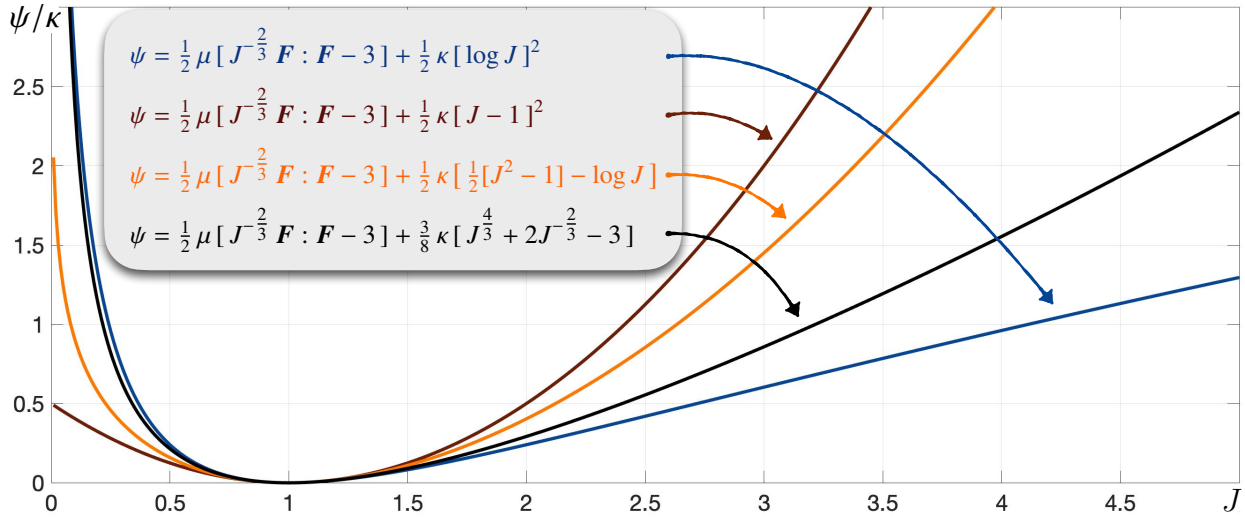

Figure 3: Comparing the volumetric term of a few free energy densities. Many of such examples have been introduced in the literature, see [46] among other. Nonetheless, we limit ourselves to these selected choices since they sufficiently introduce the problem. *The volume-preserving part is not a part of discussion here and is thus omitted for the sake of comparison by setting $\mu = 0$ for all the energies.* Note that the vertical axis shows the *dimensionless* free energy densities normalized by κ.

$\kappa/\mu \geq 2/3$. Henceforth, we define the normalized bulk modulus $K := \kappa/\mu$. That is

$$K := \kappa/\mu \quad , \quad \nu = \frac{3K-2}{6K+2} \quad \Rightarrow \quad \nu \geq 0 \quad \Leftrightarrow \quad K \geq 2/3 \quad , \quad \nu \to 1/2 \quad \Leftrightarrow \quad K \to \infty\,. \tag{22}$$

For the free energy density (21), the normalized Piola stress reads

$$\frac{\boldsymbol{P}}{\mu} = J^{-\frac{2}{3}}\,[\,\boldsymbol{F} - \frac{1}{3}\,\boldsymbol{F} : \boldsymbol{F}\,\boldsymbol{F}^{-\mathrm{t}}\,] + K\,\log J\,\boldsymbol{F}^{-\mathrm{t}}\,. \tag{23}$$

For a uniaxial tension test, with the deformation gradient $\boldsymbol{F} = \mathrm{Diag}(\lambda, \eta, \eta)$, the lateral components of Piola stress must vanish identically to satisfy the traction free boundary conditions. This results in

$$\frac{1}{3}\,J^{-\frac{2}{3}}\,[\,\eta^2 - \lambda^2\,] + K\,\log J \doteq 0 \qquad \text{with} \qquad J = \lambda\,\eta^2\,, \tag{24}$$

which can be expressed in a compact form as $f(\eta; K, \lambda)$=0 indicating that for any prescribed K and λ, we can solve for η such that the traction free boundary conditions associated with a uniaxial tension test are fulfilled. Figure 4 illustrate the solution of $f(\eta; K, \lambda)$=0 for the Flory-type free energy density of interest here, and for various values of K though all corresponding to $\nu \geq 0$. We intentionally study the material behavior in a fairly compressible regime and can immediately see that when increasing K, i.e. moving towards incompressibility, the material behavior tends to become physically more sound. In fact, the behavior of a fully compressible material with $\nu = 0$ or equivalently

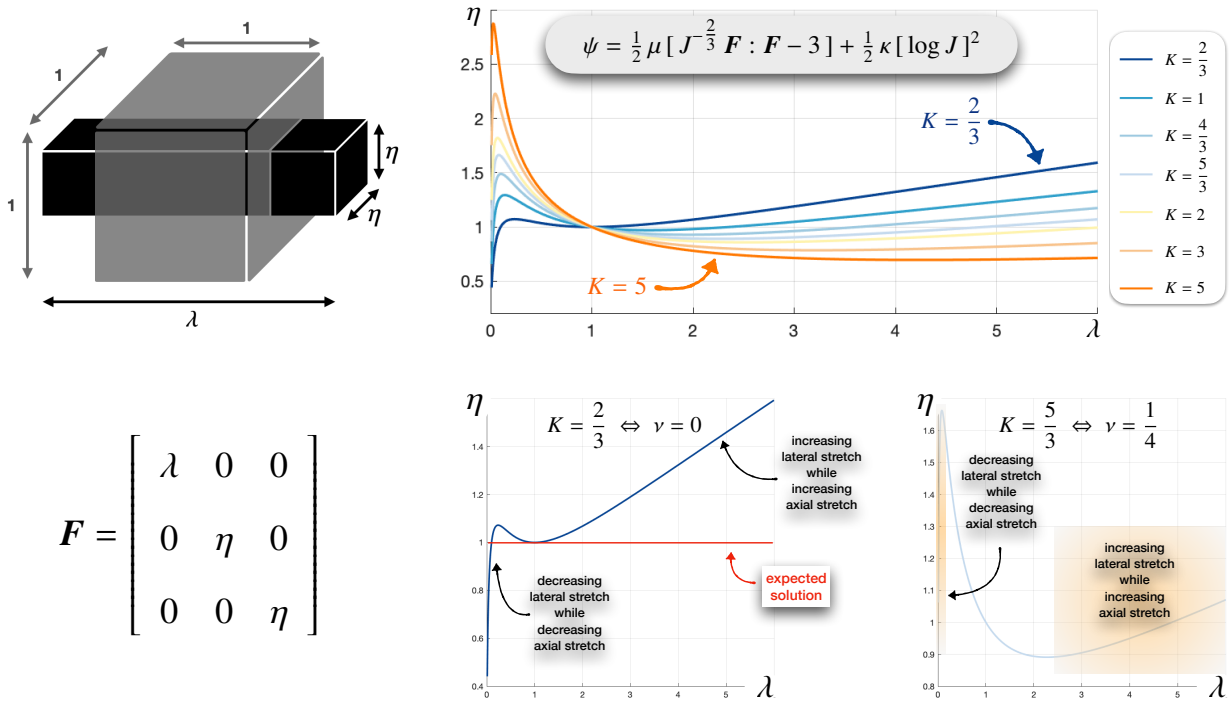

Figure 4: Affine deformation of a unit cube via the linear deformation map $\boldsymbol{F}$ for a three-dimensional uniaxial test (right). Extensional and lateral stretches are denoted as λ and η, respectively. Lateral stretch η are computed for axial stretches λ and for various compressibility ratios defined by $K = \kappa/\mu$ with $K = 2/3$ indicating a fully compressible domain ($\nu = 0$) and $K \to \infty$ indicating an incompressible domain ($\nu \to 0.5$). The results correspond to the Flory-type energy density (21).

$K = 2/3$ predicted by the Flory-type energy density is entirely unphysical. Even though for the Poisson ratio of $\nu = 0.25$ we observe a physically meaningful response in the vicinity of the reference configuration, at large stretches for both tension and compression we can see that the material behaves in an unexpected manner. We emphasize that we are in particular interested in the behavior of materials under large compressions, due to its increasing applications related to instabilities due to compressive stresses in the domain, see [48, 49] and references therein among many others.

Having established the issue with additive decomposition of free energy densities into volume-preserving and volumetric parts for the Flory-type free energy density, now we illustrate that a similar material response is obtained for the first three free energy densities in Fig. 3, however, the last energy density [45] circumvents the problem. Figure 5 depicts η versus λ for various free energy densities. The figure shows that all the energies except for the last one results in lateral contraction under axial contraction, which is not physically sound. Also, at the fully compressible limit ($\nu = 0$) associated with $K = 2/3$ all the energies except for the last one result in lateral deformation which is not expected. More precisely, *none of the commonly accepted free energy densities can recover an apparent zero Poisson's ratio*, except for the last one [45]. Table 1 gathers the Piola stress $\boldsymbol{P}$ and Piola tangent $\mathbb{A}$ with respect

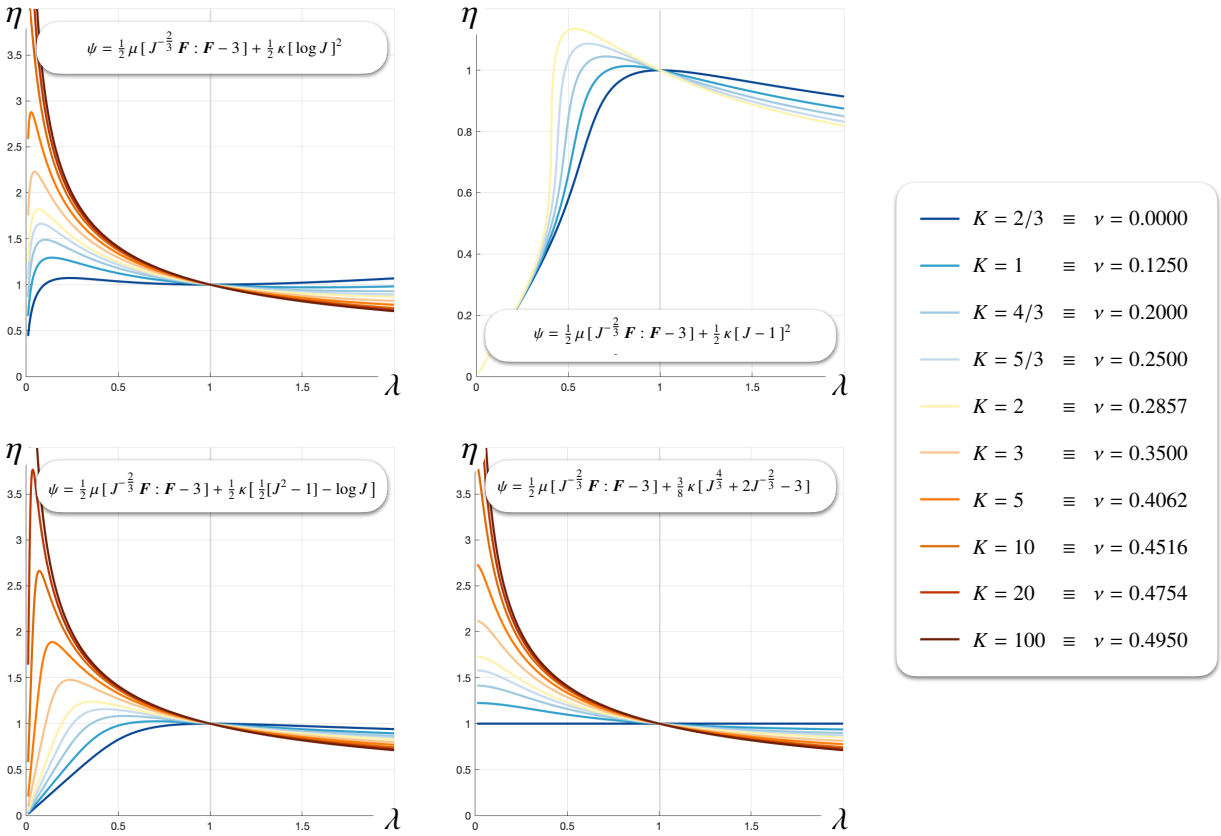

Figure 5: Lateral stretch η versus axial stretches λ and for various compressibility ratios defined by $K = \kappa/\mu$ with $K = 2/3$ indicating a fully compressible domain ($\nu = 0$) and $K \to \infty$ indicating an incompressible domain ($\nu \to 0.5$). The results correspond to the commonly accepted free energy densities in Fig. 3. Poisson's ratio is related to K via the relation $\nu = [3K - 2]/[6K + 2]$.

to $\boldsymbol{F}$ - needed for computational simulations of the examples - wherein the fourth-order tensors $\mathbb{D} := -\boldsymbol{F}^{-t} \underline{\otimes} \boldsymbol{F}^{-1}$, $\mathbb{E} := \boldsymbol{F}^{-t} \otimes \boldsymbol{F}^{-t}$, $\mathbb{G} := \boldsymbol{F} \otimes \boldsymbol{F}^{-t}$, $\mathbb{H} := \boldsymbol{F}^{-t} \otimes \boldsymbol{F}$ and $\mathbb{I} := \boldsymbol{I} \overline{\otimes} \boldsymbol{I}$ are defined to present the tangents more concisely.

Remark. The reported unphysical behavior under the simple extension test is caused by an *inappropriate* decomposition of the free energy density. Various common non-additive energy densities do not lead to this unphysical behavior but they cause numerical issues close to the incompressibility limit, e.g. in computational simulations with FEM. On the other hand, commonly accepted additively decomposed free energy densities can alleviate the numerical issues close to the incompressibility limit, but they lead to the reported unphysical behavior at lower Poisson's ratios, which is surprisingly highly overlooked in literature. The point of departure of this manuscript is the presupposition that one needs a model that can capture the material behavior across the entire compressibility spectrum and that - due to computational aspects - a decomposition of the free energy density into its volume-preserving and volumetric parts is required. The same comment holds for the surface too. Next, we propose a surface model that decomposes *appropriately* the surface free energy density into area-preserving and area-varying parts, such that it does not result

Table 1: The free energy densities in Fig. 3 together with their corresponding Piola stress $\boldsymbol{P}$ and Piola tangent $\mathbb{A}$ with respect to $\boldsymbol{F}$.

$$
\begin{aligned}
&\psi = \tfrac{1}{2}\mu\,[\,J^{-\frac{2}{3}}\,\boldsymbol{F} : \boldsymbol{F} - 3\,] + \tfrac{1}{2}\kappa\,[\,\log J\,]^2\,,\\
&\boldsymbol{P} = \mu\,J^{-\frac{2}{3}}\,[\boldsymbol{F} - \frac{1}{3}\boldsymbol{F} : \boldsymbol{F}\,\boldsymbol{F}^{-\mathrm{t}}] + \kappa\,\log J\,\boldsymbol{F}^{-\mathrm{t}}\,,\\
&\mathbb{A} = -\tfrac{2}{3}\mu\,J^{-\frac{2}{3}}\,[\mathbb{G} - \tfrac{1}{3}\boldsymbol{F} : \boldsymbol{F}\,\mathbb{E}\,] + \mu\,J^{-\frac{2}{3}}[\,\mathbb{I} - \tfrac{2}{3}\,\mathbb{H} - \tfrac{1}{3}\boldsymbol{F} : \boldsymbol{F}\,\mathbb{D}\,] + \kappa\,\log J\,\mathbb{D} + \kappa\,\mathbb{E}\,.
\end{aligned}

$$
\begin{aligned}
&\psi = \tfrac{1}{2}\mu\,[\,J^{-\frac{2}{3}}\,\boldsymbol{F} : \boldsymbol{F} - 3\,] + \tfrac{1}{2}\kappa\,[\,J - 1\,]^2\,,\\
&\boldsymbol{P} = \mu\,J^{-\frac{2}{3}}\,[\boldsymbol{F} - \tfrac{1}{3}\boldsymbol{F} : \boldsymbol{F}\,\boldsymbol{F}^{-\mathrm{t}}] + \kappa\,[J^2 - J]\,\boldsymbol{F}^{-\mathrm{t}}\,,\\
&\mathbb{A} = -\tfrac{2}{3}\mu\,J^{-\frac{2}{3}}\,[\mathbb{G} - \tfrac{1}{3}\boldsymbol{F} : \boldsymbol{F}\,\mathbb{E}\,] + \mu\,J^{-\frac{2}{3}}[\,\mathbb{I} - \tfrac{2}{3}\,\mathbb{H} - \tfrac{1}{3}\boldsymbol{F} : \boldsymbol{F}\,\mathbb{D}\,] + \kappa\,[J^2 - J]\,\mathbb{D} + \kappa\,[2J^2 - J]\,\mathbb{E}\,.
\end{aligned}
\tag{25}
$$

$$
\begin{aligned}
&\psi = \tfrac{1}{2}\mu\,[\,J^{-\frac{2}{3}}\,\boldsymbol{F} : \boldsymbol{F} - 3\,] + \tfrac{1}{2}\kappa\,[\,\tfrac{1}{2}[J^2 - 1] - \log J\,]\,,\\
&\boldsymbol{P} = \mu\,J^{-\frac{2}{3}}\,[\boldsymbol{F} - \tfrac{1}{3}\boldsymbol{F} : \boldsymbol{F}\,\boldsymbol{F}^{-\mathrm{t}}] + \tfrac{1}{2}\kappa\,[J^2 - 1]\,\boldsymbol{F}^{-\mathrm{t}}\,,\\
&\mathbb{A} = -\tfrac{2}{3}\mu\,J^{-\frac{2}{3}}\,[\mathbb{G} - \tfrac{1}{3}\boldsymbol{F} : \boldsymbol{F}\,\mathbb{E}\,] + \mu\,J^{-\frac{2}{3}}[\,\mathbb{I} - \tfrac{2}{3}\,\mathbb{H} - \tfrac{1}{3}\boldsymbol{F} : \boldsymbol{F}\,\mathbb{D}\,] + \tfrac{1}{2}\kappa\,[J^2 - 1]\,\mathbb{D} + \kappa\,J^2\,\mathbb{E}\,.
\end{aligned}

$$
\begin{aligned}
&\psi = \tfrac{1}{2}\mu\,[\,J^{-\frac{2}{3}}\boldsymbol{F} : \boldsymbol{F} - 3\,] + \tfrac{3}{8}\kappa\,[\,J^{\frac{4}{3}} + 2J^{-\frac{2}{3}} - 3\,]\,,\\
&\boldsymbol{P} = \mu\,J^{-\frac{2}{3}}\,[\boldsymbol{F} - \tfrac{1}{3}\boldsymbol{F} : \boldsymbol{F}\,\boldsymbol{F}^{-\mathrm{t}}] + \tfrac{1}{2}\kappa\,[J^{\frac{4}{3}} - J^{-\frac{2}{3}}]\,\boldsymbol{F}^{-\mathrm{t}}\,,\\
&\mathbb{A} = -\tfrac{2}{3}\mu\,J^{-\frac{2}{3}}\,[\mathbb{G} - \tfrac{1}{3}\boldsymbol{F} : \boldsymbol{F}\,\mathbb{E}\,] + \mu\,J^{-\frac{2}{3}}[\,\mathbb{I} - \tfrac{2}{3}\,\mathbb{H} - \tfrac{1}{3}\boldsymbol{F} : \boldsymbol{F}\,\mathbb{D}\,] + \tfrac{1}{2}\kappa\,[J^{\frac{4}{3}} - J^{-\frac{2}{3}}]\,\mathbb{D} + \tfrac{1}{3}\kappa\,[2J^{\frac{4}{3}} + J^{-\frac{2}{3}}]\,\mathbb{E}\,.
\end{aligned}
$$

in unphysical material behavior for any surface Poisson's ratio.

3.2. Constitutive modeling of the surface

Now, we aim to establish a surface elasticity model that is additively decomposed into area-preserving and area-varying parts. For the sake of completeness, we include a few intuitive models that mimic the structure of the first three bulk energies gathered in Fig. 3 and show that these intuitive extensions, analogously to their bulk counterparts, suffer from the issue that they result in unphysical material behavior under uniaxial tension tests. Note that despite this shortcoming, similarly to the bulk, such surface free energy densities are indeed employed in literature, e.g. [50]. Finally, we propose a proper split of the surface energy density that rectifies the problem associated with the previously introduced models.

Note that we focus on the *elastic part* of the surface free energy density that vanishes at the reference configuration. For any of the given surface free energy densities, one can add a *surface tension* part too by incorporating a constant

surface energy $\hat{\gamma}$ per area in the current configuration. When doing so, the total surface energy density $\hat{\psi}^{\text{tot}}$ can be written as

$$\hat{\psi}^{\text{tot}} = \hat{\psi} + \hat{\gamma}\,\hat{J} \qquad \text{with} \qquad \hat{\gamma} : \text{surface tension} \qquad \text{and} \qquad \hat{J} := \hat{\text{Det}}\hat{\boldsymbol{F}}\,, \tag{26}$$

with the corresponding *total* surface Piola stress $\hat{\boldsymbol{P}}^{\text{tot}}$ and its tangent $\hat{\mathbb{A}}^{\text{tot}}$ being

$$\hat{\boldsymbol{P}}^{\text{tot}} := \hat{\boldsymbol{P}} + \hat{\gamma}\,\hat{J}\,\hat{\boldsymbol{F}}^{-\text{t}} \quad \Rightarrow \quad \hat{\mathbb{A}}^{\text{tot}} := \hat{\mathbb{A}} + \hat{\gamma}\,\hat{J}\,[\hat{\mathbb{E}} + \hat{\mathbb{D}}] \qquad \text{with} \qquad \hat{\boldsymbol{P}} = \frac{\partial \hat{\psi}}{\partial \hat{\boldsymbol{F}}} \quad \text{and} \quad \hat{\mathbb{A}} = \frac{\partial \hat{\boldsymbol{P}}}{\partial \hat{\boldsymbol{F}}}\,, \tag{27}$$

where

$$\hat{\mathbb{D}} := -\hat{\boldsymbol{F}}^{-\text{t}} \underline{\otimes} \hat{\boldsymbol{F}}^{-1} + [\hat{\boldsymbol{n}} \otimes \hat{\boldsymbol{n}}] \overline{\otimes} [\hat{\boldsymbol{F}}^{-1} \cdot \hat{\boldsymbol{F}}^{-\text{t}}] \qquad \text{and} \qquad \hat{\mathbb{E}} := \hat{\boldsymbol{F}}^{-\text{t}} \otimes \hat{\boldsymbol{F}}^{-\text{t}}\,. \tag{28}$$

For the elastic part of surface free energy densities, we investigate the following models, thereby the first three mimic the structure of their bulk counterparts and *the last one is our proposition* to obtain a physically meaningful surface energy decomposition.

$$\begin{aligned}
\hat{\psi} &= \tfrac{1}{2}\,\hat{\mu}\,[\,\hat{J}^{-1}\,\hat{\boldsymbol{F}} : \hat{\boldsymbol{F}} - 2\,] + \tfrac{1}{2}\,\hat{\kappa}\,[\,\log \hat{J}\,]^2\,,\\
\hat{\psi} &= \tfrac{1}{2}\,\hat{\mu}\,[\,\hat{J}^{-1}\,\hat{\boldsymbol{F}} : \hat{\boldsymbol{F}} - 2\,] + \tfrac{1}{2}\,\hat{\kappa}\,[\,\hat{J} - 1\,]^2\,,\\
\hat{\psi} &= \tfrac{1}{2}\,\hat{\mu}\,[\,\hat{J}^{-1}\,\hat{\boldsymbol{F}} : \hat{\boldsymbol{F}} - 2\,] + \tfrac{1}{2}\,\hat{\kappa}\,[\,\tfrac{1}{2}[\hat{J}^2 - 1] - \log \hat{J}\,]\,,\\
\hat{\psi} &= \tfrac{1}{2}\,\hat{\mu}\,[\,\hat{J}^{-1}\hat{\boldsymbol{F}} : \hat{\boldsymbol{F}} - 2\,] + \tfrac{1}{2}\,\hat{\kappa}\,[\,\hat{J} + \hat{J}^{-1} - 2\,]\,.
\end{aligned} \tag{29}$$

In surface free energy densities (29), the material parameters $\hat{\mu}$ and $\hat{\kappa}$ are the surface shear and surface area moduli, respectively. For two-dimensional isotropic surface elasticity, at the reference configuration, the Poisson ratio $\hat{\nu}$ can be related to $\hat{\mu}$ and $\hat{\kappa}$ according to

$$\hat{\nu} = \frac{\hat{\kappa} - \hat{\mu}}{\hat{\kappa} + \hat{\mu}} \qquad \Rightarrow \qquad \hat{\nu} = \frac{\hat{\kappa}/\hat{\mu} - 1}{\hat{\kappa}/\hat{\mu} + 1} \qquad \Rightarrow \qquad \hat{\nu} = \frac{\hat{K} - 1}{\hat{K} + 1} \qquad \text{with} \qquad \hat{K} := \hat{\kappa}/\hat{\mu}\,, \tag{30}$$

which immediately results in

$$\hat{\nu} \geq 0 \quad \Leftrightarrow \quad \hat{K} \geq 1 \qquad , \qquad \hat{\nu} \to 1 \quad \Leftrightarrow \quad \hat{K} \to \infty\,. \tag{31}$$

Note that *the upper limit of two-dimensional Poisson's ratio associated with surface incompressibility is one and not*

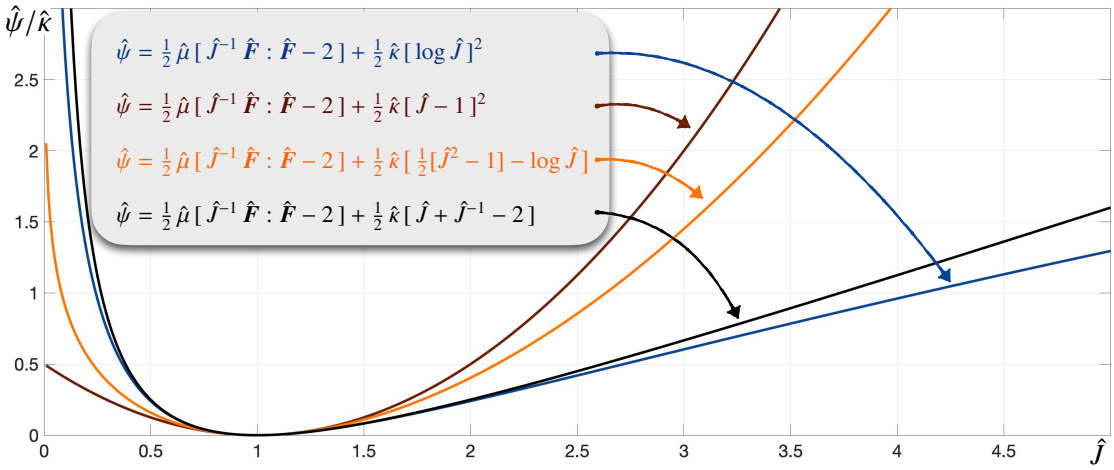

Figure 6: Comparing the surface-varying term of the surface free energy densities (29). *The area-preserving part is not a part of discussion here and is thus omitted for the sake of comparison by setting $\hat{\mu} = 0$ for all the surface energies.* Note that the vertical axis shows the *dimensionless* surface free energy densities normalized by $\hat{\kappa}$.

one-half. For a two-dimensional uniaxial tension test, with the deformation gradient $\hat{\boldsymbol{F}} = \mathrm{Diag}(\hat{\lambda}, \hat{\eta})$, the lateral stretch $\hat{\eta}$ relates to the axial stretch $\hat{\lambda}$ and the surface Poisson ratio via the relation $\hat{\eta} = \hat{\lambda}^{-\hat{\nu}}$. For the surface free energy densities (29), the surface Piola stresses read

$$
\begin{aligned}
\hat{\boldsymbol{P}} &= \hat{\mu}\,\hat{J}^{-1}\,[\,\hat{\boldsymbol{F}} - \tfrac{1}{2}\,\hat{\boldsymbol{F}} : \hat{\boldsymbol{F}}\,\hat{\boldsymbol{F}}^{-\mathrm{t}}\,] + \hat{\kappa}\,\log\hat{J}\,\hat{\boldsymbol{F}}^{-\mathrm{t}}\,,\\
\hat{\boldsymbol{P}} &= \hat{\mu}\,\hat{J}^{-1}\,[\,\hat{\boldsymbol{F}} - \tfrac{1}{2}\,\hat{\boldsymbol{F}} : \hat{\boldsymbol{F}}\,\hat{\boldsymbol{F}}^{-\mathrm{t}}\,] + \hat{\kappa}\,[\,\hat{J}^2 - \hat{J}\,]\,\hat{\boldsymbol{F}}^{-\mathrm{t}}\,,\\
\hat{\boldsymbol{P}} &= \hat{\mu}\,\hat{J}^{-1}\,[\,\hat{\boldsymbol{F}} - \tfrac{1}{2}\,\hat{\boldsymbol{F}} : \hat{\boldsymbol{F}}\,\hat{\boldsymbol{F}}^{-\mathrm{t}}\,] + \tfrac{1}{2}\,\hat{\kappa}\,[\,\hat{J}^2 - 1\,]\,\hat{\boldsymbol{F}}^{-\mathrm{t}}\,,\\
\hat{\boldsymbol{P}} &= \hat{\mu}\,\hat{J}^{-1}\,[\,\hat{\boldsymbol{F}} - \tfrac{1}{2}\,\hat{\boldsymbol{F}} : \hat{\boldsymbol{F}}\,\hat{\boldsymbol{F}}^{-\mathrm{t}}\,] + \tfrac{1}{2}\,\hat{\kappa}\,[\,\hat{J} - \hat{J}^{-1}\,]\,\hat{\boldsymbol{F}}^{-\mathrm{t}}\,.
\end{aligned}
\tag{32}
$$

Note that all the energies are identical in their area-preserving counterpart and differ only in the area-varying parts. Under a uniaxial tension of the surface, the traction free boundary condition requires $\hat{\boldsymbol{P}} \cdot \tilde{\boldsymbol{N}} = \boldsymbol{0}$ thereby $\tilde{\boldsymbol{N}}$ is the unit normal vector in $\hat{\eta}$ direction. Therefore the associated traction free conditions, remembering that $\hat{K} := \hat{\kappa}/\hat{\mu}$, read

$$
\begin{aligned}
&\hat{J}^{-1}\,[\,\hat{\eta}^2 - \hat{\lambda}^2\,] + 2\,\hat{K}\,\log\hat{J} \doteq 0 \qquad \text{with} \qquad \hat{J} = \hat{\lambda}\,\hat{\eta}\,,\\
&\hat{J}^{-1}\,[\,\hat{\eta}^2 - \hat{\lambda}^2\,] + 2\,\hat{K}\,[\,\hat{J}^2 - \hat{J}\,] \doteq 0 \qquad \text{with} \qquad \hat{J} = \hat{\lambda}\,\hat{\eta}\,,\\
&\hat{J}^{-1}\,[\,\hat{\eta}^2 - \hat{\lambda}^2\,] + \hat{K}\,[\,\hat{J}^2 - 1\,] \doteq 0 \qquad \text{with} \qquad \hat{J} = \hat{\lambda}\,\hat{\eta}\,,\\
&\hat{J}^{-1}\,[\,\hat{\eta}^2 - \hat{\lambda}^2\,] + \hat{K}\,[\,\hat{J} - \hat{J}^{-1}\,] \doteq 0 \qquad \text{with} \qquad \hat{J} = \hat{\lambda}\,\hat{\eta}\,,
\end{aligned}
\tag{33}
$$

all of which can be expressed in a compact form as $f(\hat{\eta}; \hat{K}, \hat{\lambda})$=0 indicating that for any prescribed $\hat{K}$ and $\hat{\lambda}$, we can solve for $\hat{\eta}$ such that the traction free boundary conditions associated with a uniaxial tension test are fulfilled. As we

will see shortly, all the options except for the last one result in unphysical behavior at lower Poisson's ratios. This shortcoming becomes more evident at the limit of full compressibility corresponding to $\hat{\nu} = 0$. We further analyze the last relationship $(33)_4$ that is of particular interest here since it is our proposition. After some mathematical steps, one can show that

$$\hat{J}^{-1}\,[\,\hat{\eta}^2 - \hat{\lambda}^2\,] + \hat{K}\,[\,\hat{J} - \hat{J}^{-1}\,] \doteq 0 \quad \Rightarrow \quad \hat{\eta}^2 = \frac{\hat{\lambda}^2 + \hat{K}}{\hat{K}\,\hat{\lambda}^2 + 1} \qquad \text{or} \qquad \hat{\lambda}^{-2\hat{\nu}} = \frac{\hat{\lambda}^2 + \hat{K}}{\hat{K}\,\hat{\lambda}^2 + 1}\,, \tag{34}$$

where the alternative representation is obtained using a nonlinear definition of Poisson's ratio $\hat{\eta} = \hat{\lambda}^{-\hat{\nu}}$. At the limits of full compressibility ($\hat{K} = 0$) and incompressibility ($\hat{K} \to \infty$), we therefore have

$$\begin{cases} \hat{K} = 0 \quad \Rightarrow \quad \hat{\eta} = 1 \quad \forall \hat{\lambda} \quad \Rightarrow \quad \hat{\nu} = 0.0\,, \\ \hat{K} \to \infty \quad \Rightarrow \quad \hat{\eta} = 1/\hat{\lambda} \quad \forall \hat{\lambda} \quad \Rightarrow \quad \hat{\nu} \to 1.0\,, \end{cases} \tag{35}$$

that are physically meaningful, though none of the remaining surface energy densities can satisfy condition $(35)_1$.

Figure 7 depicts $\hat{\eta}$ versus $\hat{\lambda}$ for all the introduced free energy densities. The figure shows that all the energies except for the last one results in lateral contraction under axial compression, which is not physically sound. Most importantly, at the fully compressible limit ($\hat{\nu} = 0$) associated with $\hat{K} = 1$ all the energies except for the last one result in lateral deformation which is not expected. *Except the last surface energy density that is our current proposition, none of the commonly accepted free energy densities can recover an apparent zero Poisson's ratio*. It must be noted that all these energy densities can be successfully implemented in a finite element package and the results can be obtained numerically as well as analytically. However, for computational simulations of zero-thickness surfaces under compression, surface instabilities can occur in principle [48, 51]. This aspect is yet another reason to avoid surface energy densities that result in spurious surface compressions, since they in turn cause entirely unphysical instabilities. The associated surface Piola tangents $\hat{\mathbb{A}}$ read

$$\begin{aligned} \hat{\mathbb{A}} &= \hat{\mu}\,\hat{J}^{-1}\,[\,\hat{\mathbb{I}} - \hat{\mathbb{G}} - \hat{\mathbb{H}}\,] - \tfrac{1}{2}\,\hat{\mu}\,\hat{J}^{-1}\,\hat{\boldsymbol{F}} : \hat{\boldsymbol{F}}\,[\,\hat{\mathbb{D}} - \hat{\mathbb{E}}\,] + \hat{\kappa}\,\log\hat{J}\,\hat{\mathbb{D}} + \hat{\kappa}\,\hat{\mathbb{E}}\,, \\ \hat{\mathbb{A}} &= \hat{\mu}\,\hat{J}^{-1}\,[\,\hat{\mathbb{I}} - \hat{\mathbb{G}} - \hat{\mathbb{H}}\,] - \tfrac{1}{2}\,\hat{\mu}\,\hat{J}^{-1}\,\hat{\boldsymbol{F}} : \hat{\boldsymbol{F}}\,[\,\hat{\mathbb{D}} - \hat{\mathbb{E}}\,] + \hat{\kappa}\,[\hat{J}^2 - \hat{J}]\,\hat{\mathbb{D}} + \hat{\kappa}\,[2\hat{J}^2 - \hat{J}]\,\hat{\mathbb{E}}\,, \\ \hat{\mathbb{A}} &= \hat{\mu}\,\hat{J}^{-1}\,[\,\hat{\mathbb{I}} - \hat{\mathbb{G}} - \hat{\mathbb{H}}\,] - \tfrac{1}{2}\,\hat{\mu}\,\hat{J}^{-1}\,\hat{\boldsymbol{F}} : \hat{\boldsymbol{F}}\,[\,\hat{\mathbb{D}} - \hat{\mathbb{E}}\,] + \tfrac{1}{2}\,\hat{\kappa}\,[J^2 - 1]\,\hat{\mathbb{D}} + \hat{\kappa}\,\hat{J}^2\,\hat{\mathbb{E}}\,, \\ \hat{\mathbb{A}} &= \hat{\mu}\,\hat{J}^{-1}\,[\,\hat{\mathbb{I}} - \hat{\mathbb{G}} - \hat{\mathbb{H}}\,] - \tfrac{1}{2}\,\hat{\mu}\,\hat{J}^{-1}\,\hat{\boldsymbol{F}} : \hat{\boldsymbol{F}}\,[\,\hat{\mathbb{D}} - \hat{\mathbb{E}}\,] + \tfrac{1}{2}\,\hat{\kappa}\,[\,\hat{J} - \hat{J}^{-1}\,]\,\hat{\mathbb{D}} + \tfrac{1}{2}\,\hat{\kappa}\,[\,\hat{J} + \hat{J}^{-1}\,]\,\hat{\mathbb{E}}\,, \end{aligned} \tag{36}$$

wherein the fourth-order tensors $\hat{\mathbb{G}} := \hat{\boldsymbol{F}} \otimes \hat{\boldsymbol{F}}^{-\mathrm{t}}$, $\hat{\mathbb{H}} := \hat{\boldsymbol{F}}^{-\mathrm{t}} \otimes \hat{\boldsymbol{F}}$ and $\hat{\mathbb{I}} := \boldsymbol{I} \overline{\otimes} \hat{\boldsymbol{I}}$ are defined to present the tangents more concisely.

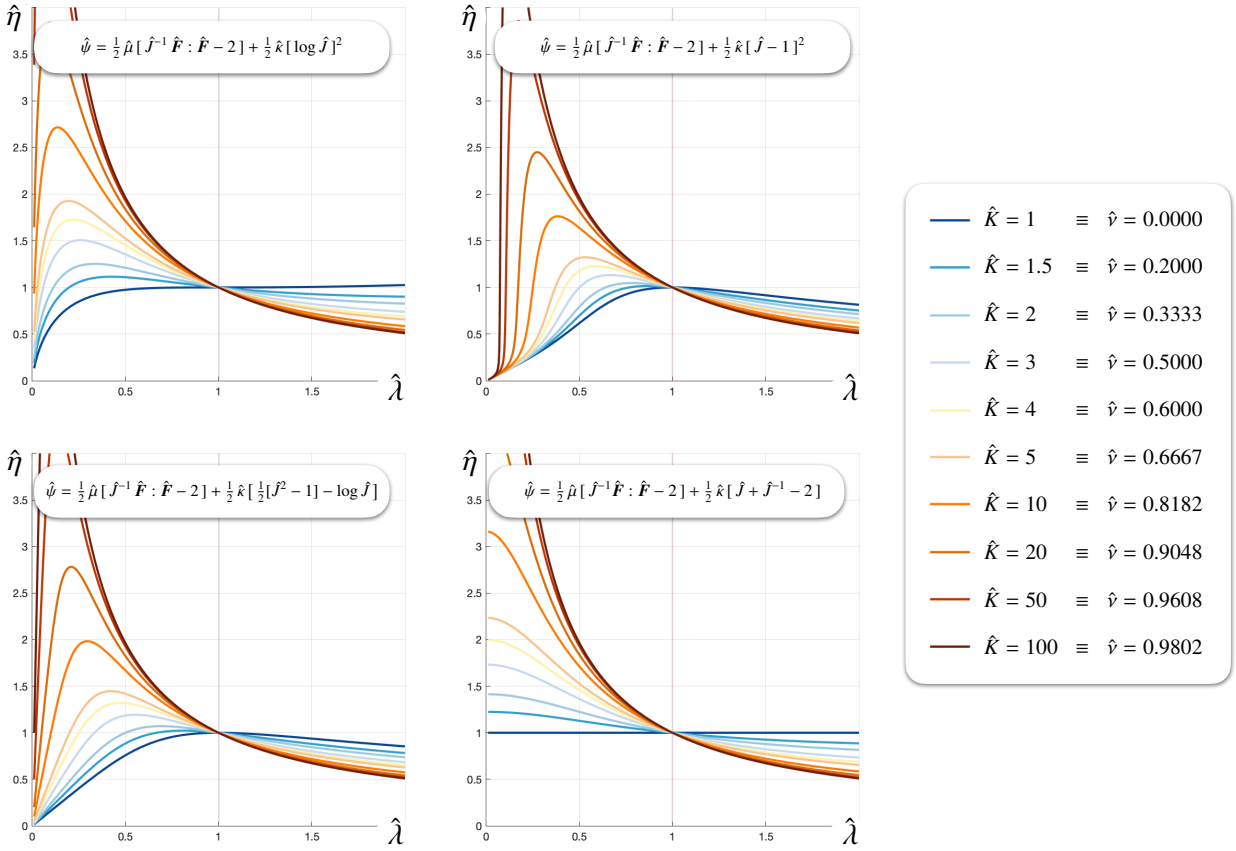

Figure 7: Lateral stretch $\hat{\eta}$ versus axial stretches $\hat{\lambda}$ and for various compressibility ratios defined by $\hat{K} = \hat{\kappa}/\hat{\mu}$ with $\hat{K} = 1$ indicating a fully compressible surface ($\hat{\nu} = 0$) and $\hat{K} \to \infty$ indicating an incompressible surface ($\hat{\nu} \to 1.0$). The results correspond to the commonly accepted free energy densities 6. Poisson's ratio is related to K via the relation $\hat{\nu} = [\hat{K} - 1]/[\hat{K} + 1]$.

4. Axi-symmetric formulation

Equipped with the three-dimensional formulation of the problem accounting for elastocapillary in Section 3, we now follow analogous steps to formulate the axisymmetric counterpart of the framework. Again, we begin with the (internal) energy Ψ that we seek to minimize. In this section, however, the energy arguments are the axisymmetric components of $\boldsymbol{F}$ and $\hat{\boldsymbol{F}}$, namely $\mathcal{F}, \zeta, \hat{\mathcal{F}}$ and $\hat{\zeta}$, instead of $\boldsymbol{F}$ and $\hat{\boldsymbol{F}}$ themselves. That is

$$\Psi = \int_{\mathscr{A}_0} \psi \, 2\pi H \, \mathrm{d}A + \int_{\partial\mathscr{A}_0} \hat{\psi} \, 2\pi \hat{H} \, \mathrm{d}L \qquad \text{with} \qquad \psi = \psi(\mathcal{F}, \zeta) \quad \text{and} \quad \hat{\psi} = \hat{\psi}(\hat{\mathcal{F}}, \hat{\zeta}) \,. \tag{37}$$

Again, the residual (10) is expressed using the chain rule as

$$\begin{aligned} \boldsymbol{R}^I &= \int_{\mathscr{A}_0} \frac{\partial \psi}{\partial \boldsymbol{\varphi}^i} \, H \, \mathrm{d}A + \int_{\partial\mathscr{A}_0} \frac{\partial \hat{\psi}}{\partial \boldsymbol{\varphi}^i} \, \hat{H} \, \mathrm{d}L \\ &= \int_{\mathscr{A}_0} \boldsymbol{\mathcal{P}} : \frac{\partial \boldsymbol{F}}{\partial \boldsymbol{\varphi}^i} \, H \, \mathrm{d}A + \int_{\mathscr{A}_0} \mathcal{S} \, \frac{\partial \zeta}{\partial \boldsymbol{\varphi}^i} \, H \, \mathrm{d}A + \int_{\partial\mathscr{A}_0} \hat{\boldsymbol{\mathcal{P}}} : \frac{\partial \hat{\boldsymbol{F}}}{\partial \boldsymbol{\varphi}^i} \, \hat{H} \, \mathrm{d}L + \int_{\partial\mathscr{A}_0} \hat{\mathcal{S}} \frac{\partial \hat{\zeta}}{\partial \boldsymbol{\varphi}^i} \, \hat{H} \, \mathrm{d}L \,, \end{aligned} \tag{38}$$

with the Piola stresses and stress-like quantities in the bulk and on the surface defined by

$$\boldsymbol{\mathcal{P}} := \frac{\partial \psi}{\partial \boldsymbol{\mathcal{F}}} \quad , \quad \mathcal{S} := \frac{\partial \psi}{\partial \zeta} \qquad \text{and} \qquad \hat{\boldsymbol{\mathcal{P}}} := \frac{\partial \hat{\psi}}{\partial \hat{\boldsymbol{\mathcal{F}}}} \quad , \quad \hat{\mathcal{S}} := \frac{\partial \hat{\psi}}{\partial \hat{\zeta}} \,. \tag{39}$$

Note that, for the sake of simplicity, we have omitted the constant coefficient 2π consistently as we aim to set the residual to zero. As assumed previously, illustrated in Fig. 2, the "two-dimensional" domain corresponding to an axisymmetric problem is on the plane orthogonal to $\boldsymbol{e}_3$. Furthermore, the unit basis vector of the symmetry axis is $\boldsymbol{e}_1$. In a near identical fashion to the three-dimensional case, the discretized forms of the deformation gradient in the bulk and on the surface follows from the shape functions, albeit on the two-dimensional domain. That is

$$\begin{aligned}
&\text{in } \mathscr{A}_0 \quad : \quad \boldsymbol{\varphi} = N^i \, \boldsymbol{\varphi}^i \quad \Rightarrow \quad \boldsymbol{\mathcal{F}} = \boldsymbol{\varphi}^i \otimes \text{Grad} N^i \quad \Rightarrow \quad \frac{\partial \boldsymbol{\mathcal{F}}}{\partial \boldsymbol{\varphi}^i} = \boldsymbol{i} \,\overline{\otimes}\, \text{Grad} N^i \,, \\
&\text{on } \partial\mathscr{A}_0 \quad : \quad \boldsymbol{\varphi} = \hat{N}^i \, \boldsymbol{\varphi}^i \quad \Rightarrow \quad \hat{\boldsymbol{\mathcal{F}}} = \boldsymbol{\varphi}^i \otimes \hat{\text{Grad}} \hat{N}^i \quad \Rightarrow \quad \frac{\partial \hat{\boldsymbol{\mathcal{F}}}}{\partial \boldsymbol{\varphi}^i} = \boldsymbol{i} \,\overline{\otimes}\, \hat{\text{Grad}} \hat{N}^i \,.
\end{aligned} \tag{40}$$

The same holds for the discretization of ζ and $\hat{\zeta}$ using the shape functions. That is

$$\begin{aligned}
&\text{in } \mathscr{A}_0 \quad : \quad \zeta = \frac{h}{H} \quad \Rightarrow \quad \zeta = N^i \left[\frac{h}{H}\right]^i \quad \Rightarrow \quad \frac{\partial \zeta}{\partial \boldsymbol{\varphi}^i} = \frac{1}{H} N^i \, \boldsymbol{e}_2 \,, \\
&\text{on } \partial\mathscr{A}_0 \quad : \quad \hat{\zeta} = \frac{\hat{h}}{\hat{H}} \quad \Rightarrow \quad \hat{\zeta} = \hat{N}^i \left[\frac{\hat{h}}{\hat{H}}\right]^i \quad \Rightarrow \quad \frac{\partial \hat{\zeta}}{\partial \boldsymbol{\varphi}^i} = \frac{1}{\hat{H}} \hat{N}^i \, \boldsymbol{e}_2 \,,
\end{aligned} \tag{41}$$

whose proof is straightforward following that $h = \boldsymbol{x} \cdot \boldsymbol{e}_2$ and $\hat{h} = \hat{\boldsymbol{x}} \cdot \boldsymbol{e}_2$ and therefore

$$\frac{\partial h^s}{\partial \boldsymbol{\varphi}^i} = \frac{\partial \boldsymbol{x}^s \cdot \boldsymbol{e}_2}{\partial \boldsymbol{\varphi}^i} = \delta_{si} \, \boldsymbol{i} \cdot \boldsymbol{e}_2 = \delta_{si} \, \boldsymbol{e}_2 \qquad \text{and} \qquad \frac{\partial \hat{h}^s}{\partial \boldsymbol{\varphi}^i} = \frac{\partial \hat{\boldsymbol{x}}^s \cdot \boldsymbol{e}_2}{\partial \boldsymbol{\varphi}^i} = \delta_{si} \, \boldsymbol{i} \cdot \boldsymbol{e}_2 = \delta_{si} \, \boldsymbol{e}_2 \,. \tag{42}$$

To proceed, it proves convenient to define the following quantities

$$\boldsymbol{\mathcal{N}}^i := \frac{1}{H} N^i \, \boldsymbol{e}_2 \qquad \text{and} \qquad \hat{\boldsymbol{\mathcal{N}}}^i := \frac{1}{\hat{H}} \hat{N}^i \, \boldsymbol{e}_2 \,. \tag{43}$$

Using the derivatives (40) and (41), together with the definitions (43), into the axisymmetric residual (38) renders

$$\boldsymbol{R}^I = \int_{\mathscr{A}_0} \boldsymbol{\mathcal{P}} \cdot \text{Grad} N^i \, H \, \mathrm{d}A + \int_{\mathscr{A}_0} \mathcal{S} \, \boldsymbol{\mathcal{N}}^i \, H \, \mathrm{d}A + \int_{\partial\mathscr{A}_0} \hat{\boldsymbol{\mathcal{P}}} \cdot \hat{\text{Grad}} \hat{N}^i \, \hat{H} \, \mathrm{d}L + \int_{\partial\mathscr{A}_0} \hat{\mathcal{S}} \, \hat{\boldsymbol{\mathcal{N}}}^i \, \hat{H} \, \mathrm{d}L \,. \tag{44}$$

Analogous to the three-dimensional framework, we assume that the global point J corresponds to its element-wise node number j and therefore, the tangent stiffness reads

$$\begin{aligned}\boldsymbol{K}^{IJ} = \frac{\partial \boldsymbol{R}^I}{\partial \boldsymbol{\varphi}^J} = &\int_{\mathscr{A}_0} \mathrm{Grad} N^i \cdot\!\cdot \frac{\partial \boldsymbol{\mathcal{P}}}{\partial \boldsymbol{\varphi}^j}\, H \,\mathrm{d}A + \int_{\mathscr{A}_0} \boldsymbol{\mathcal{N}}^i \otimes \frac{\partial \mathcal{S}}{\partial \boldsymbol{\varphi}^j}\, H \,\mathrm{d}A \\ &+ \int_{\partial\mathscr{A}_0} \hat{\mathrm{Grad}} \hat{N}^i \cdot\!\cdot \frac{\partial \hat{\boldsymbol{\mathcal{P}}}}{\partial \boldsymbol{\varphi}^j}\, \hat{H} \,\mathrm{d}L + \int_{\partial\mathscr{A}_0} \hat{\boldsymbol{\mathcal{N}}}^i \otimes \frac{\partial \hat{\mathcal{S}}}{\partial \boldsymbol{\varphi}^j}\, \hat{H} \,\mathrm{d}L\,.\end{aligned} \tag{45}$$

Now, we need to proceed using the chain-rule, though each of the quantities $\boldsymbol{\mathcal{P}}$, $\mathcal{S}$, $\hat{\boldsymbol{\mathcal{P}}}$ and $\hat{\mathcal{S}}$ are functions of two arguments. The derivatives in the first two integrals in Eq. (45) in the bulk read

$$\begin{aligned}\frac{\partial \boldsymbol{\mathcal{P}}}{\partial \boldsymbol{\varphi}^j} &= \frac{\partial \boldsymbol{\mathcal{P}}}{\partial \boldsymbol{\mathcal{F}}} : \frac{\partial \boldsymbol{\mathcal{F}}}{\partial \boldsymbol{\varphi}^j} + \frac{\partial \boldsymbol{\mathcal{P}}}{\partial \zeta} \otimes \frac{\partial \zeta}{\partial \boldsymbol{\varphi}^j} \qquad \Rightarrow \qquad \frac{\partial \boldsymbol{\mathcal{P}}}{\partial \boldsymbol{\varphi}^j} = \frac{\partial \boldsymbol{\mathcal{P}}}{\partial \boldsymbol{\mathcal{F}}} \cdot \mathrm{Grad} N^j + \frac{\partial \boldsymbol{\mathcal{P}}}{\partial \zeta} \otimes \boldsymbol{\mathcal{N}}^j\,, \\ \frac{\partial \mathcal{S}}{\partial \boldsymbol{\varphi}^j} &= \frac{\partial \mathcal{S}}{\partial \boldsymbol{\mathcal{F}}} : \frac{\partial \boldsymbol{\mathcal{F}}}{\partial \boldsymbol{\varphi}^j} + \frac{\partial \mathcal{S}}{\partial \zeta}\ \frac{\partial \zeta}{\partial \boldsymbol{\varphi}^j} \qquad \Rightarrow \qquad \frac{\partial \mathcal{S}}{\partial \boldsymbol{\varphi}^j} = \frac{\partial \mathcal{S}}{\partial \boldsymbol{\mathcal{F}}} \cdot \mathrm{Grad} N^j + \frac{\partial \mathcal{S}}{\partial \zeta}\ \boldsymbol{\mathcal{N}}^j\,.\end{aligned} \tag{46}$$

Similarly, on the surface, or rather curve on top of the planar domain, we will have

$$\begin{aligned}\frac{\partial \hat{\boldsymbol{\mathcal{P}}}}{\partial \boldsymbol{\varphi}^j} &= \frac{\partial \hat{\boldsymbol{\mathcal{P}}}}{\partial \hat{\boldsymbol{\mathcal{F}}}} : \frac{\partial \hat{\boldsymbol{\mathcal{F}}}}{\partial \boldsymbol{\varphi}^j} + \frac{\partial \hat{\boldsymbol{\mathcal{P}}}}{\partial \hat{\zeta}} \otimes \frac{\partial \hat{\zeta}}{\partial \boldsymbol{\varphi}^j} \qquad \Rightarrow \qquad \frac{\partial \hat{\boldsymbol{\mathcal{P}}}}{\partial \boldsymbol{\varphi}^j} = \frac{\partial \hat{\boldsymbol{\mathcal{P}}}}{\partial \hat{\boldsymbol{\mathcal{F}}}} \cdot \hat{\mathrm{Grad}} \hat{N}^j + \frac{\partial \hat{\boldsymbol{\mathcal{P}}}}{\partial \hat{\zeta}} \otimes \hat{\boldsymbol{\mathcal{N}}}^j\,, \\ \frac{\partial \hat{\mathcal{S}}}{\partial \boldsymbol{\varphi}^j} &= \frac{\partial \hat{\mathcal{S}}}{\partial \hat{\boldsymbol{\mathcal{F}}}} : \frac{\partial \hat{\boldsymbol{\mathcal{F}}}}{\partial \boldsymbol{\varphi}^j} + \frac{\partial \hat{\mathcal{S}}}{\partial \hat{\zeta}}\ \frac{\partial \hat{\zeta}}{\partial \boldsymbol{\varphi}^j} \qquad \Rightarrow \qquad \frac{\partial \hat{\mathcal{S}}}{\partial \boldsymbol{\varphi}^j} = \frac{\partial \hat{\mathcal{S}}}{\partial \hat{\boldsymbol{\mathcal{F}}}} \cdot \hat{\mathrm{Grad}} \hat{N}^j + \frac{\partial \hat{\mathcal{S}}}{\partial \hat{\zeta}}\ \hat{\boldsymbol{\mathcal{N}}}^j\,.\end{aligned} \tag{47}$$

Therefore, the tangent stiffness (45) for the axisymmetric framework reads

$$\begin{aligned}\boldsymbol{K}^{IJ} = &\int_{\mathscr{A}_0} \mathrm{Grad} N^i \cdot\!\cdot \boldsymbol{\mathcal{A}} \cdot \mathrm{Grad} N^j \, H \,\mathrm{d}A + \int_{\mathscr{A}_0} \mathrm{Grad} N^i \cdot\!\cdot \boldsymbol{\mathcal{B}} \otimes \boldsymbol{\mathcal{N}}^j \, H \,\mathrm{d}A \\ &+ \int_{\mathscr{A}_0} \boldsymbol{\mathcal{N}}^i \otimes \boldsymbol{\mathcal{C}} \cdot \mathrm{Grad} N^j \, H \,\mathrm{d}A + \int_{\mathscr{A}_0} \boldsymbol{\mathcal{D}}\, \boldsymbol{\mathcal{N}}^i \otimes \boldsymbol{\mathcal{N}}^j \, H \,\mathrm{d}A \\ &+ \int_{\partial\mathscr{A}_0} \hat{\mathrm{Grad}} \hat{N}^i \cdot\!\cdot \hat{\boldsymbol{\mathcal{A}}} \cdot \hat{\mathrm{Grad}} \hat{N}^j \, \hat{H} \,\mathrm{d}L + \int_{\partial\mathscr{A}_0} \hat{\mathrm{Grad}} \hat{N}^i \cdot\!\cdot \hat{\boldsymbol{\mathcal{B}}} \otimes \hat{\boldsymbol{\mathcal{N}}}^j \, \hat{H} \,\mathrm{d}L \\ &+ \int_{\partial\mathscr{A}_0} \hat{\boldsymbol{\mathcal{N}}}^i \cdot\!\cdot \hat{\boldsymbol{\mathcal{C}}} \cdot \hat{\mathrm{Grad}} \hat{N}^j \, \hat{H} \,\mathrm{d}L + \int_{\partial\mathscr{A}_0} \hat{\boldsymbol{\mathcal{D}}}\, \hat{\boldsymbol{\mathcal{N}}}^i \otimes \hat{\boldsymbol{\mathcal{N}}}^j \, \hat{H} \,\mathrm{d}L\,,\end{aligned} \tag{48}$$

wherein we have used the definitions

$$\begin{aligned}\boldsymbol{\mathcal{A}} &:= \frac{\partial \boldsymbol{\mathcal{P}}}{\partial \boldsymbol{\mathcal{F}}} \quad , \quad \boldsymbol{\mathcal{B}} := \frac{\partial \mathcal{S}}{\partial \boldsymbol{\mathcal{F}}} \quad , \quad \boldsymbol{\mathcal{C}} := \frac{\partial \boldsymbol{\mathcal{P}}}{\partial \zeta} \quad , \quad \boldsymbol{\mathcal{D}} := \frac{\partial \mathcal{S}}{\partial \zeta}\,, \\ \hat{\boldsymbol{\mathcal{A}}} &:= \frac{\partial \hat{\boldsymbol{\mathcal{P}}}}{\partial \hat{\boldsymbol{\mathcal{F}}}} \quad , \quad \hat{\boldsymbol{\mathcal{B}}} := \frac{\partial \hat{\mathcal{S}}}{\partial \hat{\boldsymbol{\mathcal{F}}}} \quad , \quad \hat{\boldsymbol{\mathcal{C}}} := \frac{\partial \hat{\boldsymbol{\mathcal{P}}}}{\partial \hat{\zeta}} \quad , \quad \hat{\boldsymbol{\mathcal{D}}} := \frac{\partial \hat{\mathcal{S}}}{\partial \hat{\zeta}}\,.\end{aligned} \tag{49}$$

The tangent stiffness (49) compared to its three-dimensional counterpart (19) has six more terms, which arise from the consistent derivations of the axisymmetric framework. Having established the final format for the residual (44) and the tangent stiffness (49), the last step is to set the free energy densities ψ in the bulk and $\hat{\psi}$ on the surface, but now in terms of $\boldsymbol{\mathcal{F}}$ and ζ in the bulk, and in terms of $\hat{\boldsymbol{\mathcal{F}}}$ and $\hat{\zeta}$ on the surface. For ψ, we employ the last option $(25)_4$ introduced for the three-dimensional framework, and derive its axisymmetric counterpart, using $\boldsymbol{F} : \boldsymbol{F} = \boldsymbol{\mathcal{F}} : \boldsymbol{\mathcal{F}} + \zeta^2$ and $J = \mathrm{Det}\boldsymbol{F} = \zeta\,\mathcal{J}$ with $\mathcal{J} := \mathrm{Det}\boldsymbol{\mathcal{F}}$. That is

$$\psi(\boldsymbol{\mathcal{F}},\zeta) = \tfrac{1}{2}\mu\,[\,\zeta^{-\frac{2}{3}}\,\mathcal{J}^{-\frac{2}{3}}\,\boldsymbol{\mathcal{F}} : \boldsymbol{\mathcal{F}} + \zeta^{\frac{4}{3}}\,\mathcal{J}^{-\frac{2}{3}} - 3\,] + \tfrac{3}{8}\kappa\,[\,\zeta^{\frac{4}{3}}\,\mathcal{J}^{\frac{4}{3}} + 2\,\zeta^{-\frac{2}{3}}\,\mathcal{J}^{-\frac{2}{3}} - 3\,]\,. \tag{50}$$

For the axisymmetric free energy density (50) the Piola stress $\boldsymbol{\mathcal{P}}$ and the stress-like quantity $\mathcal{S}$ read

$$\begin{aligned}
\boldsymbol{\mathcal{P}} &:= \frac{\partial\psi}{\partial\boldsymbol{\mathcal{F}}} = \mu\,\zeta^{-\frac{2}{3}}\,\mathcal{J}^{-\frac{2}{3}}\,\boldsymbol{\mathcal{F}} - \tfrac{1}{3}\mu\,[\,\zeta^{-\frac{2}{3}}\,\mathcal{J}^{-\frac{2}{3}}\,\boldsymbol{\mathcal{F}} : \boldsymbol{\mathcal{F}} + \zeta^{\frac{4}{3}}\,\mathcal{J}^{-\frac{2}{3}}\,]\,\boldsymbol{\mathcal{F}}^{-\mathrm{t}} + \tfrac{1}{2}\kappa\,\zeta^{-\frac{2}{3}}\,\mathcal{J}^{-\frac{2}{3}}\,[\,\zeta^2\,\mathcal{J}^2 - 1\,]\,\boldsymbol{\mathcal{F}}^{-\mathrm{t}}\,,\\
\mathcal{S} &:= \frac{\partial\psi}{\partial\zeta} = \tfrac{1}{3}\mu\,\zeta^{\frac{1}{3}}\,\mathcal{J}^{-\frac{2}{3}}\,[\,2 - \zeta^{-2}\,\boldsymbol{\mathcal{F}} : \boldsymbol{\mathcal{F}}\,] + \tfrac{1}{2}\kappa\,\zeta^{-\frac{5}{3}}\,\mathcal{J}^{-\frac{2}{3}}\,[\,\zeta^2\,\mathcal{J}^2 - 1\,]\,,
\end{aligned} \tag{51}$$

with their associated tangents

$$\begin{aligned}
\boldsymbol{\mathcal{A}} &:= \frac{\partial\boldsymbol{\mathcal{P}}}{\partial\boldsymbol{\mathcal{F}}} = \mu\,\zeta^{-\frac{2}{3}}\,\mathcal{J}^{-\frac{2}{3}}\,\mathbb{I} - \tfrac{2}{3}\mu\,\zeta^{-\frac{2}{3}}\,\mathcal{J}^{-\frac{2}{3}}\,[\,\mathbb{G} + \mathbb{H}\,]\\
&\qquad - \tfrac{1}{3}\mu\,[\,\zeta^{-\frac{2}{3}}\,\mathcal{J}^{-\frac{2}{3}}\,\boldsymbol{\mathcal{F}} : \boldsymbol{\mathcal{F}} + \zeta^{\frac{4}{3}}\,\mathcal{J}^{-\frac{2}{3}}\,]\,\mathbb{D} + \tfrac{2}{9}\mu\Big[\,\zeta^{-\frac{2}{3}}\,\mathcal{J}^{-\frac{2}{3}}\,\boldsymbol{\mathcal{F}} : \boldsymbol{\mathcal{F}} + \zeta^{\frac{4}{3}}\,\mathcal{J}^{-\frac{2}{3}}\,\Big]\,\mathbb{E}\\
&\qquad + \tfrac{1}{3}\kappa\,\zeta^{-\frac{2}{3}}\,\mathcal{J}^{-\frac{2}{3}}\,[\,2\,\zeta^2\,\mathcal{J}^2 + 1\,]\,\mathbb{E} + \tfrac{1}{2}\kappa\,\zeta^{-\frac{2}{3}}\,\mathcal{J}^{-\frac{2}{3}}\,[\,\zeta^2\,\mathcal{J}^2 - 1\,]\,\mathbb{D}\,,\\
\boldsymbol{\mathcal{B}} &:= \frac{\partial\mathcal{S}}{\partial\boldsymbol{\mathcal{F}}} = -\tfrac{2}{9}\mu\,\zeta^{\frac{1}{3}}\,\mathcal{J}^{-\frac{2}{3}}\,[\,2 - \zeta^{-2}\,\boldsymbol{\mathcal{F}} : \boldsymbol{\mathcal{F}}\,]\,\boldsymbol{\mathcal{F}}^{-\mathrm{t}} - \tfrac{2}{3}\mu\,\zeta^{-\frac{5}{3}}\,\mathcal{J}^{-\frac{2}{3}}\,\boldsymbol{\mathcal{F}} + \tfrac{1}{3}\kappa\,\zeta^{-\frac{5}{3}}\,\mathcal{J}^{-\frac{2}{3}}\,[\,2\,\zeta^2\,\mathcal{J}^2 + 1\,]\,\boldsymbol{\mathcal{F}}^{-\mathrm{t}}\,,\\
\boldsymbol{\mathcal{C}} &:= \frac{\partial\boldsymbol{\mathcal{P}}}{\partial\zeta} = -\tfrac{2}{9}\mu\,\zeta^{\frac{1}{3}}\,\mathcal{J}^{-\frac{2}{3}}\,[\,2 - \zeta^{-2}\,\boldsymbol{\mathcal{F}} : \boldsymbol{\mathcal{F}}\,]\,\boldsymbol{\mathcal{F}}^{-\mathrm{t}} - \tfrac{2}{3}\mu\,\zeta^{-\frac{5}{3}}\,\mathcal{J}^{-\frac{2}{3}}\,\boldsymbol{\mathcal{F}} + \tfrac{1}{3}\kappa\,\zeta^{-\frac{5}{3}}\,\mathcal{J}^{-\frac{2}{3}}\,[\,2\,\zeta^2\,\mathcal{J}^2 + 1\,]\,\boldsymbol{\mathcal{F}}^{-\mathrm{t}}\,,\\
\mathcal{D} &:= \frac{\partial\mathcal{S}}{\partial\zeta} = \tfrac{2}{9}\mu\,\zeta^{-\frac{2}{3}}\,\mathcal{J}^{-\frac{2}{3}} + \tfrac{5}{9}\mu\,\zeta^{-\frac{8}{3}}\,\mathcal{J}^{-\frac{2}{3}}\,\boldsymbol{\mathcal{F}} : \boldsymbol{\mathcal{F}} + \tfrac{5}{6}\kappa\,\zeta^{-\frac{8}{3}}\,\mathcal{J}^{-\frac{2}{3}} + \tfrac{1}{6}\kappa\,\zeta^{-\frac{2}{3}}\,\mathcal{J}^{\frac{4}{3}}\,,
\end{aligned} \tag{52}$$

wherein the *axisymmetric* fourth-order tensors $\mathbb{D} := -\boldsymbol{\mathcal{F}}^{-\mathrm{t}} \underline{\otimes} \boldsymbol{\mathcal{F}}^{-1}$, $\mathbb{E} := \boldsymbol{\mathcal{F}}^{-\mathrm{t}} \otimes \boldsymbol{\mathcal{F}}^{-\mathrm{t}}$, $\mathbb{G} := \boldsymbol{\mathcal{F}} \otimes \boldsymbol{\mathcal{F}}^{-\mathrm{t}}$, $\mathbb{H} := \boldsymbol{\mathcal{F}}^{-\mathrm{t}} \otimes \boldsymbol{\mathcal{F}}$ and $\mathbb{I} := \boldsymbol{\mathcal{I}} \overline{\otimes} \boldsymbol{\mathcal{I}}$, are *redefined*.

Equipped with the derivations of the free energy densities in the bulk accounting for axisymmetry, an axisymmetric surface free energy density to capture a constant surface tension is introduced next. The axisymmetric surface free energy density, in the spirit of its three-dimensional counterpart (26) reads

$$\hat{\psi}^{\mathrm{tot}}(\hat{\boldsymbol{\mathcal{F}}},\hat{\zeta}) = \hat{\psi} + \hat{\gamma}\,\hat{\mathcal{J}}\,\hat{\zeta} \qquad \text{with} \qquad \hat{\gamma} : \text{surface tension} \qquad \text{and} \qquad \hat{\mathcal{J}} := \hat{\mathrm{Det}}\hat{\boldsymbol{\mathcal{F}}}\,. \tag{53}$$

Note that $\hat{\mathcal{J}}$ essentially captures the stretch along the curve parallel to the axis of symmetry. The hoop stretch on the other hand is recovered by $\hat{\zeta}$. Therefore, the associated surface Piola stress $\hat{\boldsymbol{\mathcal{P}}}^{\text{tot}}$ and stress-like $\hat{\mathcal{S}}^{\text{tot}}$ follow as

$$\begin{aligned}
\hat{\boldsymbol{\mathcal{P}}}^{\text{tot}} &:= \frac{\partial \hat{\psi}^{\text{tot}}}{\partial \hat{\boldsymbol{\mathcal{F}}}} = \hat{\boldsymbol{\mathcal{P}}} + \hat{\gamma}\,\hat{\mathcal{J}}\,\hat{\zeta}\,\hat{\boldsymbol{\mathcal{F}}}^{-\text{t}}\,, \\
\hat{\mathcal{S}}^{\text{tot}} &:= \frac{\partial \hat{\psi}^{\text{tot}}}{\partial \hat{\zeta}} = \hat{\mathcal{S}} + \hat{\gamma}\,\hat{\mathcal{J}}\,,
\end{aligned}$$

the derivatives of which furnish the tangent stiffnesses $(49)_2$ on the surface as

$$\begin{aligned}
\hat{\boldsymbol{\mathcal{A}}}^{\text{tot}} &:= \frac{\partial \hat{\boldsymbol{\mathcal{P}}}^{\text{tot}}}{\partial \hat{\boldsymbol{\mathcal{F}}}} = \hat{\boldsymbol{\mathcal{A}}} + \hat{\gamma}\,\hat{\mathcal{J}}\,\hat{\zeta}\,\hat{\mathbb{E}} + \hat{\gamma}\,\hat{\mathcal{J}}\,\hat{\zeta}\,\hat{\mathbb{D}} \quad , \quad \hat{\boldsymbol{\mathcal{B}}}^{\text{tot}} := \frac{\partial \hat{\mathcal{S}}^{\text{tot}}}{\partial \hat{\boldsymbol{\mathcal{F}}}} = \hat{\boldsymbol{\mathcal{B}}} + \hat{\gamma}\,\hat{\mathcal{J}}\,\hat{\boldsymbol{\mathcal{F}}}^{-\text{t}}\,, \\
\hat{\boldsymbol{\mathcal{C}}}^{\text{tot}} &:= \frac{\partial \hat{\boldsymbol{\mathcal{P}}}^{\text{tot}}}{\partial \hat{\zeta}} = \hat{\boldsymbol{\mathcal{C}}} + \hat{\gamma}\,\hat{\mathcal{J}}\,\hat{\boldsymbol{\mathcal{F}}}^{-\text{t}} \quad , \quad \hat{\boldsymbol{\mathcal{D}}}^{\text{tot}} := \frac{\partial \hat{\mathcal{S}}^{\text{tot}}}{\partial \hat{\zeta}} = \hat{\boldsymbol{\mathcal{D}}}\,,
\end{aligned}$$

with $\hat{\mathbb{D}} := -\hat{\boldsymbol{\mathcal{F}}}^{-\text{t}} \underline{\otimes} \hat{\boldsymbol{\mathcal{F}}}^{-1} + [\hat{\boldsymbol{n}} \otimes \hat{\boldsymbol{n}}] \overline{\otimes} [\hat{\boldsymbol{\mathcal{F}}}^{-1} \cdot \hat{\boldsymbol{\mathcal{F}}}^{-\text{t}}]$ and $\hat{\mathbb{E}} := \hat{\boldsymbol{\mathcal{F}}}^{-\text{t}} \otimes \hat{\boldsymbol{\mathcal{F}}}^{-\text{t}}$. For the elastic part of axisymmetric surface free energy densities, we investigate the following models (29) but now we express their equivalent axisymmetric ones, using the relationships $\hat{\boldsymbol{F}} : \hat{\boldsymbol{F}} = \hat{\boldsymbol{\mathcal{F}}} : \hat{\boldsymbol{\mathcal{F}}} + \hat{\zeta}^2$ and $\hat{J} = \hat{\mathcal{J}}\,\hat{\zeta}$. That is

$$\begin{aligned}
\hat{\psi}(\hat{\boldsymbol{\mathcal{F}}}, \hat{\zeta}) &= \tfrac{1}{2}\,\hat{\mu}\,[\,\hat{\mathcal{J}}^{-1}\,\hat{\zeta}^{-1}\,[\hat{\boldsymbol{\mathcal{F}}} : \hat{\boldsymbol{\mathcal{F}}} + \hat{\zeta}^2] - 2\,] + \tfrac{1}{2}\,\hat{\kappa}\,[\,\log(\hat{\mathcal{J}}\,\hat{\zeta})\,]^2\,, \\
\hat{\psi}(\hat{\boldsymbol{\mathcal{F}}}, \hat{\zeta}) &= \tfrac{1}{2}\,\hat{\mu}\,[\,\hat{\mathcal{J}}^{-1}\,\hat{\zeta}^{-1}\,[\hat{\boldsymbol{\mathcal{F}}} : \hat{\boldsymbol{\mathcal{F}}} + \hat{\zeta}^2] - 2\,] + \tfrac{1}{2}\,\hat{\kappa}\,[\,\hat{\mathcal{J}}\,\hat{\zeta} - 1\,]^2\,, \\
\hat{\psi}(\hat{\boldsymbol{\mathcal{F}}}, \hat{\zeta}) &= \tfrac{1}{2}\,\hat{\mu}\,[\,\hat{\mathcal{J}}^{-1}\,\hat{\zeta}^{-1}\,[\hat{\boldsymbol{\mathcal{F}}} : \hat{\boldsymbol{\mathcal{F}}} + \hat{\zeta}^2] - 2\,] + \tfrac{1}{2}\,\hat{\kappa}\,[\,\tfrac{1}{2}[\hat{\mathcal{J}}^2\,\hat{\zeta}^2 - 1] - \log(\hat{\mathcal{J}}\,\hat{\zeta})\,]\,, \\
\hat{\psi}(\hat{\boldsymbol{\mathcal{F}}}, \hat{\zeta}) &= \tfrac{1}{2}\,\hat{\mu}\,[\,\hat{\mathcal{J}}^{-1}\,\hat{\zeta}^{-1}[\hat{\boldsymbol{\mathcal{F}}} : \hat{\boldsymbol{\mathcal{F}}} + \hat{\zeta}^2] - 2\,] + \tfrac{1}{2}\,\hat{\kappa}\,[\,\hat{\mathcal{J}}\,\hat{\zeta} + \hat{\mathcal{J}}^{-1}\,\hat{\zeta}^{-1} - 2\,]\,.
\end{aligned} \tag{54}$$

The surface Piola stress $\hat{\boldsymbol{\mathcal{P}}}$ and the surface stress-like quantity $\hat{\mathcal{S}}$ associated with the axisymmetric surface free energy densities (54), together with their corresponding second derivatives are given in Appendix A. We include the derivatives of the last energy density $(54)_4$ here to emphasize that it is the only one that recovers fully compressible surface behavior. That is

$$\begin{aligned}
\hat{\boldsymbol{\mathcal{P}}} &:= \frac{\partial \hat{\psi}}{\partial \hat{\boldsymbol{\mathcal{F}}}} = \hat{\mu}\,\hat{\mathcal{J}}^{-1}\,\hat{\zeta}^{-1}\,\hat{\boldsymbol{\mathcal{F}}} - \tfrac{1}{2}\,\hat{\mu}\,\hat{\mathcal{J}}^{-1}\,\hat{\zeta}^{-1}\,[\,\hat{\boldsymbol{\mathcal{F}}} : \hat{\boldsymbol{\mathcal{F}}} + \hat{\zeta}^2\,]\,\hat{\boldsymbol{\mathcal{F}}}^{-\text{t}} + \tfrac{1}{2}\,\hat{\kappa}\,[\,\hat{\mathcal{J}}\,\hat{\zeta} - \hat{\mathcal{J}}^{-1}\,\hat{\zeta}^{-1}\,]\,\hat{\boldsymbol{\mathcal{F}}}^{-\text{t}}\,, \\
\hat{\mathcal{S}} &:= \frac{\partial \hat{\psi}}{\partial \hat{\zeta}} = -\tfrac{1}{2}\,\hat{\mu}\,\hat{\mathcal{J}}^{-1}\,\hat{\zeta}^{-2}\,[\,\hat{\boldsymbol{\mathcal{F}}} : \hat{\boldsymbol{\mathcal{F}}} - \hat{\zeta}^2\,] + \tfrac{1}{2}\,\hat{\kappa}\,[\,\hat{\mathcal{J}}\,\hat{\zeta} - \hat{\mathcal{J}}^{-1}\,\hat{\zeta}^{-1}\,]\,\hat{\zeta}^{-1}\,,
\end{aligned} \tag{55}$$

and consequently

$$
\begin{aligned}
\hat{\mathcal{A}} &:= \frac{\partial \hat{\boldsymbol{\mathcal{P}}}}{\partial \hat{\boldsymbol{\mathcal{F}}}} = \hat{\mu}\,\hat{\mathcal{J}}^{-1}\,\hat{\zeta}^{-1}\,[\,\hat{\mathbb{I}} - \hat{\mathbb{G}} - \hat{\mathbb{H}}\,] - \tfrac{1}{2}\,\hat{\mu}\,\hat{\mathcal{J}}^{-1}\,\hat{\zeta}^{-1}\,[\,\hat{\boldsymbol{\mathcal{F}}} : \hat{\boldsymbol{\mathcal{F}}} + \hat{\zeta}^{2}\,]\,[\,\hat{\mathbb{D}} - \hat{\mathbb{E}}\,] \\
&\qquad + \tfrac{1}{2}\,\hat{\kappa}\,[\,\hat{\mathcal{J}}\,\hat{\zeta} - \hat{\mathcal{J}}^{-1}\,\hat{\zeta}^{-1}\,]\,\hat{\mathbb{D}} + \tfrac{1}{2}\,\hat{\kappa}\,[\,\hat{\mathcal{J}}\,\hat{\zeta} + \hat{\mathcal{J}}^{-1}\,\hat{\zeta}^{-1}\,]\,\hat{\mathbb{E}}, \\
\hat{\mathcal{B}} &:= \frac{\partial \hat{\mathcal{S}}}{\partial \hat{\boldsymbol{\mathcal{F}}}} = \tfrac{1}{2}\,\hat{\mu}\,\hat{\mathcal{J}}^{-1}\,\hat{\zeta}^{-2}\,[\,\hat{\boldsymbol{\mathcal{F}}} : \hat{\boldsymbol{\mathcal{F}}} - \hat{\zeta}^{2}\,]\,\hat{\boldsymbol{\mathcal{F}}}^{-\mathrm{t}} - \hat{\mu}\,\hat{\mathcal{J}}^{-1}\,\hat{\zeta}^{-2}\,\hat{\boldsymbol{\mathcal{F}}} + \tfrac{1}{2}\,\hat{\kappa}\,[\,\hat{\mathcal{J}}\,\hat{\zeta} + \hat{\mathcal{J}}^{-1}\,\hat{\zeta}^{-1}\,]\,\hat{\zeta}^{-1}\,\hat{\boldsymbol{\mathcal{F}}}^{-\mathrm{t}}, \\
\hat{\boldsymbol{\mathcal{C}}} &:= \frac{\partial \hat{\boldsymbol{\mathcal{P}}}}{\partial \hat{\zeta}} = -\hat{\mu}\,\hat{\mathcal{J}}^{-1}\,\hat{\zeta}^{-2}\,\hat{\boldsymbol{\mathcal{F}}} + \tfrac{1}{2}\,\hat{\mu}\,\hat{\mathcal{J}}^{-1}\,\hat{\zeta}^{-2}\,[\,\hat{\boldsymbol{\mathcal{F}}} : \hat{\boldsymbol{\mathcal{F}}} - \hat{\zeta}^{2}\,]\,\hat{\boldsymbol{\mathcal{F}}}^{-\mathrm{t}} + \tfrac{1}{2}\,\hat{\kappa}\,[\,\hat{\mathcal{J}}\,\hat{\zeta} + \hat{\mathcal{J}}^{-1}\,\hat{\zeta}^{-1}\,]\,\hat{\zeta}^{-1}\,\hat{\boldsymbol{\mathcal{F}}}^{-\mathrm{t}}, \\
\hat{\mathcal{D}} &:= \frac{\partial \hat{\mathcal{S}}}{\partial \hat{\zeta}} = \hat{\mu}\,\hat{\mathcal{J}}^{-1}\,\hat{\zeta}^{-3}\,\hat{\boldsymbol{\mathcal{F}}} : \hat{\boldsymbol{\mathcal{F}}} + \hat{\kappa}\,\hat{\mathcal{J}}^{-1}\,\hat{\zeta}^{-3}.
\end{aligned}
\tag{56}
$$

wherein the *axisymmetric* fourth-order tensors $\hat{\mathbb{G}} := \hat{\boldsymbol{\mathcal{F}}} \otimes \hat{\boldsymbol{\mathcal{F}}}^{-\mathrm{t}}$, $\hat{\mathbb{H}} := \hat{\boldsymbol{\mathcal{F}}}^{-\mathrm{t}} \otimes \hat{\boldsymbol{\mathcal{F}}}$ and $\hat{\mathbb{I}} := \boldsymbol{\mathcal{I}} \overline{\otimes} \hat{\boldsymbol{\mathcal{I}}}$, are *redefined* though using the same letters. Having established the axisymmetric framework and the novel surface energy density, together with its derivatives, finally we illustrate the theory via the numerical examples next.

5. Numerical examples

The key purpose of the numerical examples in this section is to elucidate the theory and the fact that the surface energy density $(54)_4$ is throughout numerical simulations not only a viable but also a reliable candidate to decompose the surface energy into area-preserving and area-varying part in that it furnishes physically meaningful results from fully compressible to nearly incompressible elastic surfaces at large deformations. The domain of interest here is simply a cylinder with the length-to-diameter ratio of unity under 100% tension along its symmetry axis. For the numerical examples, we prescribe Dirichlet-type boundary conditions on the sides to prescribe the aforementioned stretch of 100% while the remaining part of the surface is under homogeneous Neumann-type boundary conditions, though it is endowed with surface elasticity. Throughout the examples, we monitor the radius of the domain at its center, starting from one in the reference configuration. For the energy density of the bulk, we employ Eq. (50) and vary the Poisson ratio of the bulk from fully compressible to nearly incompressible. The ratio of $\hat{\mu}/\mu = 10$ is assumed and the corresponding $\hat{\kappa}$ and κ are calculated depending on the Poisson ratio of interest for each example.

Figure 8 depicts the deformations associated with the example for the limiting case of a fully compressible bulk and nearly incompressible surface behavior highlighted on the first graph in Fig. 9. It can be seen that the surface near incompressibility plays a significant role on the material response. Also, note that the deformation profile is qualitatively reminiscent of the well established liquid-bridge example. Though in a liquid-bridge example, the surface tension is the underlying force to minimize the surface area but here the surface incompressibility is the cause of that

wherein the surface tension is assumed to be zero.

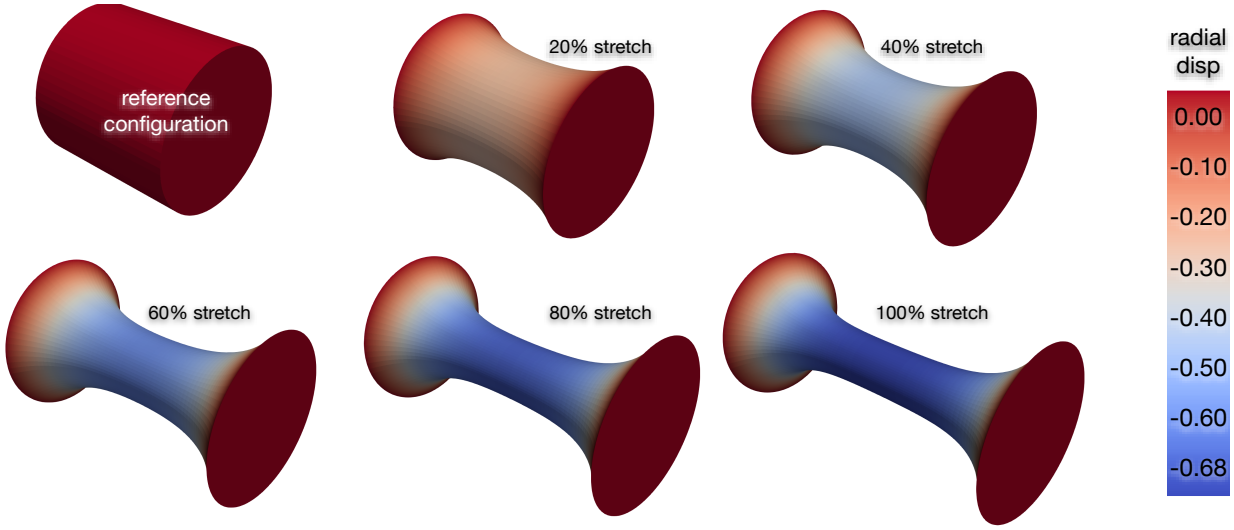

Figure 8: Deformation of a cylinder under a prescribed stretch of 100%. The colors correspond to the radial displacement at the center of the cylinder. The surface is assumed to be nearly incompressible with $\hat{K} = 100$ associated with $\hat{\nu} = 0.98$ but the bulk behaves in a fully compressible manner, highlighted on the first graph in Fig. 9. Therefore, the deformation profile is mainly dictated by the surface incompressibility.

Figure 9 illustrates the results of the numerical examples for five different Poisson's ratios in the bulk and five different Poisson's ratio of the surface. It can be clearly seen that for a fully compressible bulk and surface elasticity, the height of the domain at its center remains exactly at one, *which would have been impossible to capture with any other combination of free energy densities*. This outcome clearly elucidates the significance of the novel surface energy density $(54)_4$ proposed and investigated here, for the first time. Equally importantly, it can be seen that the proposed surface energy density captures the surface Poisson's effect and incompressibility robustly. The quadratic convergence associated with the Newton–Raphson scheme is consistently obtained at all the increments and for any combination of bulk and surface Poisson's ratios.

6. Conclusion

Motivated by the increasing interest in the surface elasticity theory of Gurtin–Murdoch for applications to soft solids such as hydrogels, we have proposed a novel constitutive model to capture surface behavior at large deformations from being fully compressible to nearly incompressible elasticity. The proposed model decomposes the surface free energy density into area-preserving and area-varying parts and therefore, it is particularly advantageous for computational implementations. The proposed form does not result in unphysical material behavior at lower Poisson's ratios, unlike other options. To elucidate the theory, and to provide a complete framework with utility to axisymmetric problems e.g. Plateau–Rayleigh instabilities, we have formulated axisymmetric problems systematically and

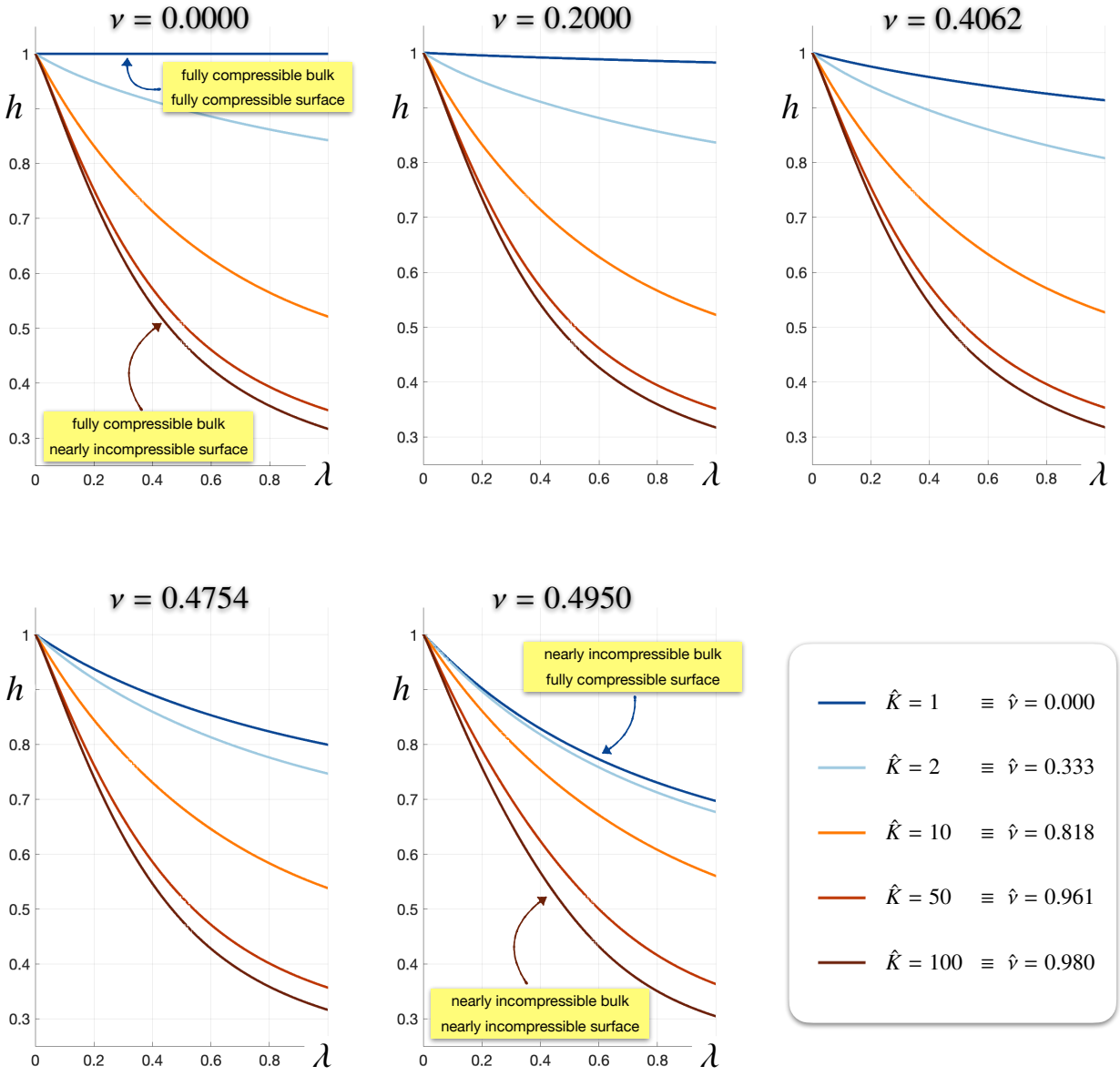

Figure 9: Radius of the domain at its center versus the prescribed stretch on its sides. Stretch of 100% corresponds to $\lambda = 1$ and the reference configuration coincides with $\lambda = 0$. Five different Poisson's ratios are considered for the bulk illustrated on five different graphs. The lines on each graph depict the five different Poisson's ratio for the surface.

employed it for computational simulations using the finite element method. The presented axisymmetric formulation complete with the novel surface constitutive model proves to be an efficient and generic tool to study elastocapillary behaviors in polymeric soft solids. Our next immediate plan is to employ the current formulation to study Plateau–Rayleigh instabilities in the spirit of our recent contribution [52].

Acknowledgment

AJ gratefully acknowledges the support provided by the Scientific and Technological Research Council of Turkey (TÜBITAK) Career Development Program, grant number 218M700. BD acknowledges funding from the National Science Foundation (NSF) through the DMREF program under grant number CMMI 2119716.

Appendix A. Axisymmetric surface energies and their associated derivatives

Here we list the derivatives of the surface free energy densities (54) for axisymmetric problems. These derivatives are useful for the computational implementation using the finite element method. We recall the definitions of the *axisymmetric* fourth-order tensors

$$\begin{aligned} &\hat{\mathbb{D}} := -\hat{\boldsymbol{\mathcal{F}}}^{-t} \underline{\otimes} \hat{\boldsymbol{\mathcal{F}}}^{-1} + [\hat{\boldsymbol{n}} \otimes \hat{\boldsymbol{n}}] \overline{\otimes} [\hat{\boldsymbol{\mathcal{F}}}^{-1} \cdot \hat{\boldsymbol{\mathcal{F}}}^{-t}] \quad , \quad \hat{\mathbb{E}} := \hat{\boldsymbol{\mathcal{F}}}^{-t} \otimes \hat{\boldsymbol{\mathcal{F}}}^{-t} , \\ &\hat{\mathbb{G}} := \hat{\boldsymbol{\mathcal{F}}} \otimes \hat{\boldsymbol{\mathcal{F}}}^{-t} \qquad\qquad\qquad\qquad , \quad \hat{\mathbb{H}} := \hat{\boldsymbol{\mathcal{F}}}^{-t} \otimes \hat{\boldsymbol{\mathcal{F}}} \qquad , \quad \hat{\mathbb{I}} := \boldsymbol{\mathcal{I}} \overline{\otimes} \hat{\boldsymbol{\mathcal{I}}} . \end{aligned} \tag{A.1}$$

Table A.2: The surface free energy density $(54)_1$ together with its corresponding derivatives with respect to $\hat{\boldsymbol{\mathcal{F}}}$ and $\hat{\zeta}$.

$$\hat{\psi} = \tfrac{1}{2}\,\hat{\mu}\,[\,\hat{\mathcal{J}}^{-1}\,\hat{\zeta}^{-1}\,[\hat{\boldsymbol{\mathcal{F}}} : \hat{\boldsymbol{\mathcal{F}}} + \hat{\zeta}^2] - 2\,] + \tfrac{1}{2}\,\hat{\kappa}\,[\,\log(\hat{\mathcal{J}}\,\hat{\zeta})\,]^2 ,$$

$$\hat{\boldsymbol{\mathcal{P}}} := \frac{\partial \hat{\psi}}{\partial \hat{\boldsymbol{\mathcal{F}}}} = \hat{\mu}\,\hat{\mathcal{J}}^{-1}\,\hat{\zeta}^{-1}\,\hat{\boldsymbol{\mathcal{F}}} - \tfrac{1}{2}\,\hat{\mu}\,\hat{\mathcal{J}}^{-1}\,\hat{\zeta}^{-1}\,[\,\hat{\boldsymbol{\mathcal{F}}} : \hat{\boldsymbol{\mathcal{F}}} + \hat{\zeta}^2\,]\,\hat{\boldsymbol{\mathcal{F}}}^{-t} + \hat{\kappa}\,\log(\hat{\mathcal{J}}\,\hat{\zeta})\,\hat{\boldsymbol{\mathcal{F}}}^{-t} ,$$

$$\hat{\mathcal{S}} := \frac{\partial \hat{\psi}}{\partial \hat{\zeta}} = -\tfrac{1}{2}\,\hat{\mu}\,\hat{\mathcal{J}}^{-1}\,\hat{\zeta}^{-2}\,[\,\hat{\boldsymbol{\mathcal{F}}} : \hat{\boldsymbol{\mathcal{F}}} - \hat{\zeta}^2\,] + \hat{\kappa}\,\log(\hat{\mathcal{J}}\,\hat{\zeta})\,\hat{\zeta}^{-1} ,$$

$$\begin{aligned} \hat{\boldsymbol{\mathcal{A}}} := \frac{\partial \hat{\boldsymbol{\mathcal{P}}}}{\partial \hat{\boldsymbol{\mathcal{F}}}} &= \hat{\mu}\,\hat{\mathcal{J}}^{-1}\,\hat{\zeta}^{-1}\,[\,\hat{\mathbb{I}} - \hat{\mathbb{G}} - \hat{\mathbb{H}}\,] - \tfrac{1}{2}\,\hat{\mu}\,\hat{\mathcal{J}}^{-1}\,\hat{\zeta}^{-1}\,[\,\hat{\boldsymbol{\mathcal{F}}} : \hat{\boldsymbol{\mathcal{F}}} + \hat{\zeta}^2\,]\,[\,\hat{\mathbb{D}} - \hat{\mathbb{E}}\,] \\ &\quad + \hat{\kappa}\,\mathbb{E} + \hat{\kappa}\,\log(\hat{\mathcal{J}}\,\hat{\zeta})\,\hat{\mathbb{D}} , \end{aligned}$$

$$\hat{\boldsymbol{\mathcal{B}}} := \frac{\partial \hat{\mathcal{S}}}{\partial \hat{\boldsymbol{\mathcal{F}}}} = \tfrac{1}{2}\,\hat{\mu}\,\hat{\mathcal{J}}^{-1}\,\hat{\zeta}^{-2}\,[\,\hat{\boldsymbol{\mathcal{F}}} : \hat{\boldsymbol{\mathcal{F}}} - \hat{\zeta}^2\,]\,\hat{\boldsymbol{\mathcal{F}}}^{-t} - \hat{\mu}\,\hat{\mathcal{J}}^{-1}\,\hat{\zeta}^{-2}\,\hat{\boldsymbol{\mathcal{F}}} + \hat{\kappa}\,\hat{\zeta}^{-1}\,\hat{\boldsymbol{\mathcal{F}}}^{-t} ,$$

$$\hat{\boldsymbol{\mathcal{C}}} := \frac{\partial \hat{\boldsymbol{\mathcal{P}}}}{\partial \hat{\zeta}} = -\hat{\mu}\,\hat{\mathcal{J}}^{-1}\,\hat{\zeta}^{-2}\,\hat{\boldsymbol{\mathcal{F}}} + \tfrac{1}{2}\,\hat{\mu}\,\hat{\mathcal{J}}^{-1}\,\hat{\zeta}^{-2}\,[\,\hat{\boldsymbol{\mathcal{F}}} : \hat{\boldsymbol{\mathcal{F}}} - \hat{\zeta}^2\,]\,\hat{\boldsymbol{\mathcal{F}}}^{-t} + \hat{\kappa}\,\hat{\zeta}^{-1}\,\hat{\boldsymbol{\mathcal{F}}}^{-t} ,$$

$$\hat{\mathcal{D}} := \frac{\partial \hat{\mathcal{S}}}{\partial \hat{\zeta}} = \hat{\mu}\,\hat{\mathcal{J}}^{-1}\,\hat{\zeta}^{-3}\,\hat{\boldsymbol{\mathcal{F}}} : \hat{\boldsymbol{\mathcal{F}}} - \hat{\kappa}\,[\,\log(\hat{\mathcal{J}}\,\hat{\zeta}) - 1\,]\,\hat{\zeta}^{-2} .$$

Table A.3: The surface free energy density $(54)_2$ together with its corresponding derivatives with respect to $\hat{\boldsymbol{\mathcal{F}}}$ and $\hat{\zeta}$.

$$\hat{\psi} = \tfrac{1}{2}\hat{\mu}\,[\,\hat{\mathcal{J}}^{-1}\,\hat{\zeta}^{-1}\,[\hat{\boldsymbol{\mathcal{F}}} : \hat{\boldsymbol{\mathcal{F}}} + \hat{\zeta}^2] - 2\,] + \tfrac{1}{2}\hat{\kappa}\,[\,\hat{\mathcal{J}}\,\hat{\zeta} - 1\,]^2\,,$$

$$\hat{\boldsymbol{\mathcal{P}}} := \frac{\partial\hat{\psi}}{\partial\hat{\boldsymbol{\mathcal{F}}}} = \hat{\mu}\,\hat{\mathcal{J}}^{-1}\,\hat{\zeta}^{-1}\,\hat{\boldsymbol{\mathcal{F}}} - \tfrac{1}{2}\hat{\mu}\,\hat{\mathcal{J}}^{-1}\,\hat{\zeta}^{-1}\,[\,\hat{\boldsymbol{\mathcal{F}}} : \hat{\boldsymbol{\mathcal{F}}} + \hat{\zeta}^2\,]\,\hat{\boldsymbol{\mathcal{F}}}^{-\mathrm{t}} + \hat{\kappa}\,[\,\hat{\mathcal{J}}\,\hat{\zeta} - 1\,]\,\hat{\mathcal{J}}\,\hat{\zeta}\,\hat{\boldsymbol{\mathcal{F}}}^{-\mathrm{t}}\,,$$

$$\hat{\mathcal{S}} := \frac{\partial\hat{\psi}}{\partial\hat{\zeta}} = -\tfrac{1}{2}\hat{\mu}\,\hat{\mathcal{J}}^{-1}\,\hat{\zeta}^{-2}\,[\,\hat{\boldsymbol{\mathcal{F}}} : \hat{\boldsymbol{\mathcal{F}}} - \hat{\zeta}^2\,] + \hat{\kappa}\,[\,\hat{\mathcal{J}}\,\hat{\zeta} - 1\,]\,\hat{\mathcal{J}}\,,$$

$$\begin{aligned}
\hat{\boldsymbol{\mathcal{A}}} := \frac{\partial\hat{\boldsymbol{\mathcal{P}}}}{\partial\hat{\boldsymbol{\mathcal{F}}}} &= \hat{\mu}\,\hat{\mathcal{J}}^{-1}\,\hat{\zeta}^{-1}\,[\,\hat{\mathbb{I}} - \hat{\mathbb{G}} - \hat{\mathbb{H}}\,] - \tfrac{1}{2}\hat{\mu}\,\hat{\mathcal{J}}^{-1}\,\hat{\zeta}^{-1}\,[\,\hat{\boldsymbol{\mathcal{F}}} : \hat{\boldsymbol{\mathcal{F}}} + \hat{\zeta}^2\,]\,[\,\hat{\mathbb{D}} - \hat{\mathbb{E}}\,] \\
&\quad + \hat{\kappa}\,[\,\hat{\mathcal{J}}\,\hat{\zeta} - 1\,]\,\hat{\mathcal{J}}\,\hat{\zeta}\,\hat{\mathbb{D}} + \hat{\kappa}\,[\,2\hat{\mathcal{J}}\,\hat{\zeta} - 1\,]\,\hat{\mathcal{J}}\,\hat{\zeta}\,\hat{\mathbb{E}}\,, \\
\hat{\boldsymbol{\mathcal{B}}} := \frac{\partial\hat{\mathcal{S}}}{\partial\hat{\boldsymbol{\mathcal{F}}}} &= \tfrac{1}{2}\hat{\mu}\,\hat{\mathcal{J}}^{-1}\,\hat{\zeta}^{-2}\,[\,\hat{\boldsymbol{\mathcal{F}}} : \hat{\boldsymbol{\mathcal{F}}} - \hat{\zeta}^2\,]\,\hat{\boldsymbol{\mathcal{F}}}^{-\mathrm{t}} - \hat{\mu}\,\hat{\mathcal{J}}^{-1}\,\hat{\zeta}^{-2}\,\hat{\boldsymbol{\mathcal{F}}} + \hat{\kappa}\,[\,2\hat{\mathcal{J}}\,\hat{\zeta} - 1\,]\,\hat{\mathcal{J}}\,\hat{\boldsymbol{\mathcal{F}}}^{-\mathrm{t}}\,, \\
\hat{\boldsymbol{\mathcal{C}}} := \frac{\partial\hat{\boldsymbol{\mathcal{P}}}}{\partial\hat{\zeta}} &= -\hat{\mu}\,\hat{\mathcal{J}}^{-1}\,\hat{\zeta}^{-2}\,\hat{\boldsymbol{\mathcal{F}}} + \tfrac{1}{2}\hat{\mu}\,\hat{\mathcal{J}}^{-1}\,\hat{\zeta}^{-2}\,[\,\hat{\boldsymbol{\mathcal{F}}} : \hat{\boldsymbol{\mathcal{F}}} - \hat{\zeta}^2\,]\,\hat{\boldsymbol{\mathcal{F}}}^{-\mathrm{t}} + \hat{\kappa}\,[\,2\hat{\mathcal{J}}\,\hat{\zeta} - 1\,]\,\hat{\mathcal{J}}\,\hat{\boldsymbol{\mathcal{F}}}^{-\mathrm{t}}\,, \\
\hat{\mathcal{D}} := \frac{\partial\hat{\mathcal{S}}}{\partial\hat{\zeta}} &= \hat{\mu}\,\hat{\mathcal{J}}^{-1}\,\hat{\zeta}^{-3}\,\hat{\boldsymbol{\mathcal{F}}} : \hat{\boldsymbol{\mathcal{F}}} + \hat{\kappa}\,\hat{\mathcal{J}}^2\,.
\end{aligned}$$

Table A.4: The surface free energy density $(54)_3$ together with its corresponding derivatives with respect to $\hat{\boldsymbol{\mathcal{F}}}$ and $\hat{\zeta}$.

$$\hat{\psi} = \tfrac{1}{2}\hat{\mu}\,[\,\hat{\mathcal{J}}^{-1}\,\hat{\zeta}^{-1}\,[\hat{\boldsymbol{\mathcal{F}}} : \hat{\boldsymbol{\mathcal{F}}} + \hat{\zeta}^2] - 2\,] + \tfrac{1}{2}\hat{\kappa}\,[\,\tfrac{1}{2}[\hat{\mathcal{J}}^2\,\hat{\zeta}^2 - 1] - \log(\hat{\mathcal{J}}\,\hat{\zeta})\,]\,,$$

$$\hat{\boldsymbol{\mathcal{P}}} := \frac{\partial\hat{\psi}}{\partial\hat{\boldsymbol{\mathcal{F}}}} = \hat{\mu}\,\hat{\mathcal{J}}^{-1}\,\hat{\zeta}^{-1}\,\hat{\boldsymbol{\mathcal{F}}} - \tfrac{1}{2}\hat{\mu}\,\hat{\mathcal{J}}^{-1}\,\hat{\zeta}^{-1}\,[\,\hat{\boldsymbol{\mathcal{F}}} : \hat{\boldsymbol{\mathcal{F}}} + \hat{\zeta}^2\,]\,\hat{\boldsymbol{\mathcal{F}}}^{-\mathrm{t}} + \tfrac{1}{2}\hat{\kappa}\,[\,\hat{\mathcal{J}}^2\,\hat{\zeta}^2 - 1\,]\,\hat{\boldsymbol{\mathcal{F}}}^{-\mathrm{t}}\,,$$

$$\hat{\mathcal{S}} := \frac{\partial\hat{\psi}}{\partial\hat{\zeta}} = -\tfrac{1}{2}\hat{\mu}\,\hat{\mathcal{J}}^{-1}\,\hat{\zeta}^{-2}\,[\,\hat{\boldsymbol{\mathcal{F}}} : \hat{\boldsymbol{\mathcal{F}}} - \hat{\zeta}^2\,] + \tfrac{1}{2}\hat{\kappa}\,[\,\hat{\mathcal{J}}^2\,\hat{\zeta}^2 - 1\,]\,\hat{\zeta}^{-1}\,,$$

$$\begin{aligned}
\hat{\boldsymbol{\mathcal{A}}} := \frac{\partial\hat{\boldsymbol{\mathcal{P}}}}{\partial\hat{\boldsymbol{\mathcal{F}}}} &= \hat{\mu}\,\hat{\mathcal{J}}^{-1}\,\hat{\zeta}^{-1}\,[\,\hat{\mathbb{I}} - \hat{\mathbb{G}} - \hat{\mathbb{H}}\,] - \tfrac{1}{2}\hat{\mu}\,\hat{\mathcal{J}}^{-1}\,\hat{\zeta}^{-1}\,[\,\hat{\boldsymbol{\mathcal{F}}} : \hat{\boldsymbol{\mathcal{F}}} + \hat{\zeta}^2\,]\,[\,\hat{\mathbb{D}} - \hat{\mathbb{E}}\,] \\
&\quad + \tfrac{1}{2}\hat{\kappa}\,[\,\hat{\mathcal{J}}^2\,\hat{\zeta}^2 - 1\,]\,\hat{\mathbb{D}} + \hat{\kappa}\,\hat{\mathcal{J}}^2\,\hat{\zeta}^2\,\hat{\mathbb{E}}\,, \\
\hat{\boldsymbol{\mathcal{B}}} := \frac{\partial\hat{\mathcal{S}}}{\partial\hat{\boldsymbol{\mathcal{F}}}} &= \tfrac{1}{2}\hat{\mu}\,\hat{\mathcal{J}}^{-1}\,\hat{\zeta}^{-2}\,[\,\hat{\boldsymbol{\mathcal{F}}} : \hat{\boldsymbol{\mathcal{F}}} - \hat{\zeta}^2\,]\,\hat{\boldsymbol{\mathcal{F}}}^{-\mathrm{t}} - \hat{\mu}\,\hat{\mathcal{J}}^{-1}\,\hat{\zeta}^{-2}\,\hat{\boldsymbol{\mathcal{F}}} + \hat{\kappa}\,\hat{\mathcal{J}}^2\,\hat{\zeta}\,\hat{\boldsymbol{\mathcal{F}}}^{-\mathrm{t}}\,, \\
\hat{\boldsymbol{\mathcal{C}}} := \frac{\partial\hat{\boldsymbol{\mathcal{P}}}}{\partial\hat{\zeta}} &= -\hat{\mu}\,\hat{\mathcal{J}}^{-1}\,\hat{\zeta}^{-2}\,\hat{\boldsymbol{\mathcal{F}}} + \tfrac{1}{2}\hat{\mu}\,\hat{\mathcal{J}}^{-1}\,\hat{\zeta}^{-2}\,[\,\hat{\boldsymbol{\mathcal{F}}} : \hat{\boldsymbol{\mathcal{F}}} - \hat{\zeta}^2\,]\,\hat{\boldsymbol{\mathcal{F}}}^{-\mathrm{t}} + \hat{\kappa}\,\hat{\mathcal{J}}^2\,\hat{\zeta}\,\hat{\boldsymbol{\mathcal{F}}}^{-\mathrm{t}}\,, \\
\hat{\mathcal{D}} := \frac{\partial\hat{\mathcal{S}}}{\partial\hat{\zeta}} &= \hat{\mu}\,\hat{\mathcal{J}}^{-1}\,\hat{\zeta}^{-3}\,\hat{\boldsymbol{\mathcal{F}}} : \hat{\boldsymbol{\mathcal{F}}} + \tfrac{1}{2}\hat{\kappa}\,[\,\hat{\mathcal{J}}^2 + \hat{\zeta}^{-2}\,]\,.
\end{aligned}$$

Table A.5: The surface free energy density $(54)_4$ together with its corresponding derivatives with respect to $\hat{\boldsymbol{\mathcal{F}}}$ and $\hat{\zeta}$.

$$\hat{\psi} = \tfrac{1}{2}\,\hat{\mu}\,[\,\hat{\mathcal{J}}^{-1}\,\hat{\zeta}^{-1}[\hat{\boldsymbol{\mathcal{F}}} : \hat{\boldsymbol{\mathcal{F}}} + \hat{\zeta}^2] - 2\,] + \tfrac{1}{2}\,\hat{\kappa}\,[\,\hat{\mathcal{J}}\,\hat{\zeta} + \hat{\mathcal{J}}^{-1}\,\hat{\zeta}^{-1} - 2\,],$$

$$\hat{\boldsymbol{\mathcal{P}}} := \frac{\partial\hat{\psi}}{\partial\hat{\boldsymbol{\mathcal{F}}}} = \hat{\mu}\,\hat{\mathcal{J}}^{-1}\,\hat{\zeta}^{-1}\,\hat{\boldsymbol{\mathcal{F}}} - \tfrac{1}{2}\,\hat{\mu}\,\hat{\mathcal{J}}^{-1}\,\hat{\zeta}^{-1}\,[\,\hat{\boldsymbol{\mathcal{F}}} : \hat{\boldsymbol{\mathcal{F}}} + \hat{\zeta}^2\,]\,\hat{\boldsymbol{\mathcal{F}}}^{-\mathrm{t}} + \tfrac{1}{2}\,\hat{\kappa}\,[\,\hat{\mathcal{J}}\,\hat{\zeta} - \hat{\mathcal{J}}^{-1}\,\hat{\zeta}^{-1}\,]\,\hat{\boldsymbol{\mathcal{F}}}^{-\mathrm{t}},$$

$$\hat{\mathcal{S}} := \frac{\partial\hat{\psi}}{\partial\hat{\zeta}} = -\tfrac{1}{2}\,\hat{\mu}\,\hat{\mathcal{J}}^{-1}\,\hat{\zeta}^{-2}\,[\,\hat{\boldsymbol{\mathcal{F}}} : \hat{\boldsymbol{\mathcal{F}}} - \hat{\zeta}^2\,] + \tfrac{1}{2}\,\hat{\kappa}\,[\,\hat{\mathcal{J}}\,\hat{\zeta} - \hat{\mathcal{J}}^{-1}\,\hat{\zeta}^{-1}\,]\,\hat{\zeta}^{-1},$$

$$\begin{aligned}\hat{\boldsymbol{\mathcal{A}}} := \frac{\partial\hat{\boldsymbol{\mathcal{P}}}}{\partial\hat{\boldsymbol{\mathcal{F}}}} &= \hat{\mu}\,\hat{\mathcal{J}}^{-1}\,\hat{\zeta}^{-1}\,[\,\hat{\mathbb{I}} - \hat{\mathbb{G}} - \hat{\mathbb{H}}\,] - \tfrac{1}{2}\,\hat{\mu}\,\hat{\mathcal{J}}^{-1}\,\hat{\zeta}^{-1}\,[\,\hat{\boldsymbol{\mathcal{F}}} : \hat{\boldsymbol{\mathcal{F}}} + \hat{\zeta}^2\,]\,[\,\hat{\mathbb{D}} - \hat{\mathbb{E}}\,] \\ &\quad + \tfrac{1}{2}\,\hat{\kappa}\,[\,\hat{\mathcal{J}}\,\hat{\zeta} - \hat{\mathcal{J}}^{-1}\,\hat{\zeta}^{-1}\,]\,\hat{\mathbb{D}} + \tfrac{1}{2}\,\hat{\kappa}\,[\,\hat{\mathcal{J}}\,\hat{\zeta} + \hat{\mathcal{J}}^{-1}\,\hat{\zeta}^{-1}\,]\,\hat{\mathbb{E}},\end{aligned}$$

$$\hat{\boldsymbol{\mathcal{B}}} := \frac{\partial\hat{\mathcal{S}}}{\partial\hat{\boldsymbol{\mathcal{F}}}} = \tfrac{1}{2}\,\hat{\mu}\,\hat{\mathcal{J}}^{-1}\,\hat{\zeta}^{-2}\,[\,\hat{\boldsymbol{\mathcal{F}}} : \hat{\boldsymbol{\mathcal{F}}} - \hat{\zeta}^2\,]\,\hat{\boldsymbol{\mathcal{F}}}^{-\mathrm{t}} - \hat{\mu}\,\hat{\mathcal{J}}^{-1}\,\hat{\zeta}^{-2}\,\hat{\boldsymbol{\mathcal{F}}} + \tfrac{1}{2}\,\hat{\kappa}\,[\,\hat{\mathcal{J}}\,\hat{\zeta} + \hat{\mathcal{J}}^{-1}\,\hat{\zeta}^{-1}\,]\,\hat{\zeta}^{-1}\,\hat{\boldsymbol{\mathcal{F}}}^{-\mathrm{t}},$$

$$\hat{\boldsymbol{\mathcal{C}}} := \frac{\partial\hat{\boldsymbol{\mathcal{P}}}}{\partial\hat{\zeta}} = -\hat{\mu}\,\hat{\mathcal{J}}^{-1}\,\hat{\zeta}^{-2}\,\hat{\boldsymbol{\mathcal{F}}} + \tfrac{1}{2}\,\hat{\mu}\,\hat{\mathcal{J}}^{-1}\,\hat{\zeta}^{-2}\,[\,\hat{\boldsymbol{\mathcal{F}}} : \hat{\boldsymbol{\mathcal{F}}} - \hat{\zeta}^2\,]\,\hat{\boldsymbol{\mathcal{F}}}^{-\mathrm{t}} + \tfrac{1}{2}\,\hat{\kappa}\,[\,\hat{\mathcal{J}}\,\hat{\zeta} + \hat{\mathcal{J}}^{-1}\,\hat{\zeta}^{-1}\,]\,\hat{\zeta}^{-1}\,\hat{\boldsymbol{\mathcal{F}}}^{-\mathrm{t}},$$

$$\hat{\mathcal{D}} := \frac{\partial\hat{\mathcal{S}}}{\partial\hat{\zeta}} = \hat{\mu}\,\hat{\mathcal{J}}^{-1}\,\hat{\zeta}^{-3}\,\hat{\boldsymbol{\mathcal{F}}} : \hat{\boldsymbol{\mathcal{F}}} + \hat{\kappa}\,\hat{\mathcal{J}}^{-1}\,\hat{\zeta}^{-3}.$$

References

[1] C. W. Barney, C. E. Dougan, K. R. McLeod, A. Kazemi-Moridani, Y. Zheng, Z. Ye, S. Tiwari, I. Sacligil, R. A. Riggleman, S. Cai, J.-H. Lee, S. R. Peyton, G. N. Tew, A. J. Crosby, Cavitation in soft matter, Proceedings of the National Academy of Sciences 117 (2020) 9157–9165.

[2] R. W. Style, R. Boltyanskiy, B. Allen, K. E. Jensen, H. P. Foote, J. S. Wettlaufer, E. R. Dufresne, Stiffening solids with liquid inclusions, Nature Physics 11 (2015) 82–87.

[3] N. Kazem, M. D. Bartlett, C. Majidi, Extreme Toughening of Soft Materials with Liquid Metal, Advanced Materials 30 (2018) 1706594.

[4] J. Dervaux, M. Roché, L. Limat, Nonlinear theory of wetting on deformable substrates, Soft Matter 16 (2020) 5157–5176.

[5] B. Andreotti, J. H. Snoeijer, Soft wetting and the Shuttleworth effect, at the crossroads between thermodynamics and mechanics, EPL (Europhysics Letters) 113 (2016) 66001.

[6] J. B. Bostwick, M. Shearer, K. E. Daniels, Elastocapillary deformations on partially-wetting substrates: Rival contact-line models, Soft Matter 10 (2014) 7361–7369.

[7] W. Zhao, J. Zhou, H. Hu, C. Xu, Q. Xu, The role of crosslinking density in surface stress and surface energy of soft solids, Soft Matter 18 (2022) 507–513.

[8] J. T. Pham, F. Schellenberger, M. Kappl, H.-J. Butt, From elasticity to capillarity in soft materials indentation, Physical Review Materials 1 (2017) 015602.

[9] C.-Y. Hui, T. Liu, T. Salez, E. Raphael, A. Jagota, Indentation of a rigid sphere into an elastic substrate with surface tension and adhesion, Proceedings of the Royal Society A: Mathematical, Physical and Engineering Sciences 471 (2015) 20140727. doi:10.1098/rspa.2014.0727.

[10] T. Liu, R. Long, C.-Y. Hui, The energy release rate of a pressurized crack in soft elastic materials: Effects of surface tension and large deformation, Soft Matter 10 (2014) 7723–7729.

[11] D. P. Holmes, P.-T. Brun, A. Pandey, S. Protière, Rising beyond elastocapillarity, Soft Matter 12 (2016) 4886–4890.

[12] Q. Liu, T. Ouchi, L. Jin, R. Hayward, Z. Suo, Elastocapillary Crease, Physical Review Letters 122 (2019) 098003.

[13] L. E. Scriven, Dynamics of a fluid interface Equation of motion for Newtonian surface fluids, Chemical Engineering Science 12 (1960) 98–108.

[14] M. E. Gurtin, A. Ian Murdoch, A continuum theory of elastic material surfaces, Archive for Rational Mechanics and Analysis 57 (1975) 291–323.

[15] P. Sharma, S. Ganti, N. Bhate, Effect of surfaces on the size-dependent elastic state of nano-inhomogeneities, Applied Physics Letters 82 (2003) 535–537.

[16] R. Dingreville, J. Qu, Mohammed Cherkaoui, Surface free energy and its effect on the elastic behavior of nano-sized particles, wires and films, Journal of the Mechanics and Physics of Solids 53 (2005) 1827–1854.

[17] J. He, C. M. Lilley, Surface effect on the elastic behavior of static bending nanowires, Nano Letters 8 (2008) 1798–1802.

[18] H. L. Duan, J. Wang, B. L. Karihaloo, Theory of Elasticity at the Nanoscale, Advances in Applied Mechanics 42 (2009) 1–68.

[19] A. Javili, A. McBride, P. Steinmann, Thermomechanics of solids with lower-dimensional energetics: On the importance of surface, interface, and curve structures at the nanoscale. A unifying review, Applied Mechanics Reviews 65 (2013) 010802.

[20] J. Yvonnet, H. L. Quang, Q. C. He, An XFEM/level set approach to modelling surface/interface effects and to computing the size-dependent effective properties of nanocomposites, Computational Mechanics 42 (2008) 119–131.

[21] A. Javili, A. Mcbride, J. Mergheim, P. Steinmann, U. Schmidt, Micro-to-macro transitions for continua with surface structure at the microscale, International Journal of Solids and Structures 50 (2013) 2561–2572.

[22] A. Javili, G. Chatzigeorgiou, A. T. McBride, P. Steinmann, C. Linder, Computational homogenization of nano-materials accounting for size effects via surface elasticity, GAMM Mitteilungen 38 (2015) 285–312.

[23] H. S. Park, P. A. Klein, G. J. Wagner, A surface Cauchy-Born model for nanoscale materials, International Journal for Numerical Methods in Engineering 68 (2006) 1072–1095.

[24] H. S. Park, P. A. Klein, A Surface Cauchy-Born model for silicon nanostructures, Computer Methods in Applied Mechanics and Engineering 197 (2008) 3249–3260.

[25] J. Yvonnet, A. Mitrushchenkov, G. Chambaud, Q. C. He, Finite element model of ionic nanowires with size-dependent mechanical properties determined by ab initio calculations, Computer Methods in Applied Mechanics and Engineering 200 (2011) 614–625.

[26] D. Davydov, A. Javili, P. Steinmann, On molecular statics and surface-enhanced continuum modeling of nano-structures, Computational Materials Science 69 (2013) 510–519.

[27] P. H. Saksono, D. Perić, On finite element modelling of surface tension Variational formulation and applications - Part I: Quasistatic problems, Computational Mechanics 38 (2006) 265–281.

[28] P. H. Saksono, D. Perić, On finite element modelling of surface tension: Variational formulation and applications - Part II: Dynamic problems, Computational Mechanics 38 (2006) 251–263.

[29] R. Brown, F. Orr, L. Scriven, Static drop on an inclined plate: Analysis by the finite element method, Journal of Colloid and Interface Science (1980) 76–87.

[30] A. Javili, P. Steinmann, A finite element framework for continua with boundary energies. Part I: The two-dimensional case, Computer Methods in Applied Mechanics and Engineering 198 (2009) 2198–2208.

[31] A. Javili, P. Steinmann, A finite element framework for continua with boundary energies. Part II: The three-dimensional case, Computer Methods in Applied Mechanics and Engineering 199 (2010) 755–765.

[32] D. L. Henann, K. Bertoldi, Modeling of elasto-capillary phenomena, Soft Matter 10 (2014) 709–717.

[33] Y. Wang, D. L. Henann, Finite-element modeling of soft solids with liquid inclusions, Extreme Mechanics Letters 9 (2016) 147–157.

[34] S. Mora, C. Maurini, T. Phou, J.-M. Fromental, B. Audoly, Y. Pomeau, Solid Drops: Large Capillary Deformations of Immersed Elastic Rods, Physical Review Letters 111 (2013) 114301.

[35] J. He, H. S. Park, A methodology for modeling surface effects on stiff and soft solids, Computational Mechanics 61 (2018) 687–697.

[36] S. Seifi, H. S. Park, Electro-elastocapillary Rayleigh-plateau instability in dielectric elastomer films, Soft Matter 13 (2017) 4305–4310.

[37] R. W. Style, A. Jagota, C.-Y. Hui, E. R. Dufresne, Elastocapillarity: Surface Tension and the Mechanics of Soft Solids, Annual Review of Condensed Matter Physics 8 (2017) 99–118.

[38] A. I. Murdoch, A thermodynamical theory of elastic material interfaces, Quarterly Journal of Mechanics and Applied Mathematics 29 (1976) 245–275.

[39] F. Dell'isola, A. Romano, On the derivation of thermomechanical balance equations for continuous systems with a nonmaterial interface, International Journal of Engineering Science 25 (1987) 1459–1468.

[40] D. J. Steigmann, R. W. Ogden, Elastic surface-substrate interactions, Proceedings of the Royal Society A: Mathematical, Physical and Engineering Sciences 455 (1999) 437–474.

[41] E. Fried, M. E. Gurtin, Thermomechanics of the interface between a body and its environment, Continuum Mechanics and Thermodynamics 19 (2007) 253–271.

[42] R. A. Sauer, R. Ghaffari, A. Gupta, The multiplicative deformation split for shells with application to growth, chemical swelling, thermoelasticity, viscoelasticity and elastoplasticity, International Journal of Solids and Structures 174-175 (2019) 53–68.

[43] B. Dortdivanlioglu, A. Javili, Boundary viscoelasticity theory at finite deformations and computational implementation using isogeometric analysis, Computer Methods in Applied Mechanics and Engineering 374 (2021) 113579.

[44] W. Ehlers, G. Eipper, The simple tension problem at large volumetric strains computed from finite hyperelastic material laws, Acta Mechanica

130 (1998) 17–27.

[45] B. Nedjar, On constitutive models of finite elasticity with possible zero apparent Poisson's ratio, International Journal of Solids and Structures 91 (2016) 72–77.

[46] S. Hartmann, P. Neff, Polyconvexity of generalized polynomial-type hyperelastic strain energy functions for near-incompressibility, International Journal of Solids and Structures 40 (11) (2003) 2767–2791.

[47] P. Neff, I.-d. Ghiba, J. Lankeit, The Exponentiated Hencky-Logarithmic Strain Energy . Part I : Constitutive Issues and Rank-One Convexity, J Elast (2015) 143–234doi:10.1007/s10659-015-9524-7.

[48] A. D. Bakiler, B. Dortdivanlioglu, A. Javili, From beams to bilayers: A unifying approach towards instabilities of compressible domains under plane deformations, International Journal of Non-Linear Mechanics 135 (2021) 103752.

[49] A. D. Bakiler, A. Javili, Wrinkling of a compressible trilayer domain under large plane deformations, International Journal of Solids and Structures 241 (2022) 111465.

[50] R. A. Sauer, T. X. Duong, K. K. Mandadapu, D. J. Steigmann, A stabilized finite element formulation for liquid shells and its application to lipid bilayers, Journal of Computational Physics 330 (2017) 436–466.

[51] A. Javili, A. McBride, P. Steinmann, B. D. Reddy, Relationships between the admissible range of surface material parameters and stability of linearly elastic bodies, Philosophical Magazine 92 (2012) 3540–3563.

[52] B. Dortdivanlioglu, A. Javili, Plateau Rayleigh instability of soft elastic solids. Effect of compressibility on pre and post bifurcation behavior, Extreme Mechanics Letters 55 (2022) 101797.